Degradation of Glycocalyx and Multiple Manifestations of Endothelial Dysfunction Coincide in the Early Phase of Endothelial Dysfunction Before Atherosclerotic Plaque Development in Apolipoprotein E/Low-Density Lipoprotein Receptor-Deficient Mice

Anna Bar, MSc; Marta Targosz-Korecka, PhD; Joanna Suraj, MSc; Bartosz Proniewski, PhD; Agnieszka Jasztal, MSc; Brygida Marczyk, MSc; Magdalena Sternak, PhD; Magdalena Przybyło, PhD; Anna Kurpińska, PhD; Maria Walczak, PhD; Renata B. Kostogrys, PhD; Marek Szymonski, PhD; Stefan Chlopicki, MD, PhD

Background—The impairment of endothelium-dependent vasodilation, increased endothelial permeability, and glycocalyx degradation are all important pathophysiological components of endothelial dysfunction. However, it is still not clear whether in atherosclerosis, glycocalyx injury precedes other features of endothelial dysfunction or these events coincide.

Methods and Results—Herein, we demonstrate that in 4- to 8-week-old apolipoprotein E/low-density lipoprotein receptor-deficient mice, at the stage before development of atherosclerotic plaques, impaired acetylcholine-induced vasodilation, reduced NO production in aorta, and increased endothelial permeability were all observed; however, flow-mediated dilation in the femoral artery was fully preserved. In 4-week-old mice, glycocalyx coverage was reduced and endothelial stiffness was increased, whereas glycocalyx length was significantly decreased at 8 weeks of age. Early changes in endothelial function were also featured by increased plasma concentration of biomarkers of glycocalyx disruption (endocan), biomarkers of endothelial inflammation (soluble vascular cell adhesion molecule 1), increased vascular permeability (angiopoietin 2), and alterations in hemostasis (tissue plasminogen activator and plasminogen activator inhibitor 1). In 28-week-old mice, at the stage of advanced atherosclerotic plaque development, impaired NO production and nearly all other features of endothelial dysfunction were changed to a similar extent, compared with the preatherosclerotic plaque phase. The exceptions were the occurrence of acetylcholine-induced vasoconstriction in the aorta and brachiocephalic artery, impaired flow-mediated vasodilation in the femoral artery, and further reduction of glycocalyx length and coverage with a concomitant further increase in endothelial permeability.

Conclusions—In conclusion, even at the early stage before the development of atherosclerotic plaques, endothelial dysfunction is a complex multifactorial response that has not been previously appreciated. (***J Am Heart Assoc***. 2019;8:e011171. DOI: 10. 1161/JAHA.118.011171.)

Key Words: atherosclerosis • atomic force microscopy • endothelial function • glycocalyx • magnetic resonance imaging

The maintenance of vascular homeostasis is accomplished through the vascular endothelium, which is responsible for regulation of many processes, including vascular tone and permeability, smooth muscle cell proliferation and migration, thromboresistance, fibrinolysis, and inflammation.[1,2] Endothelial dysfunction is a hallmark of various

Clinical Perspective

What Is New?

- In the present study in apolipoprotein E/low-density lipoprotein receptor-deficient mice, state-of-the-art in vivo magnetic resonance imaging–based methods and various ex vivo analytical techniques were used to characterize multiple manifestations of the early phase of endothelial dysfunction that emerged as a complex and multifactorial response, hitherto not appreciated.
- We demonstrated that glycocalyx injury coincided with the impairment of endothelium-dependent vasodilation and NO-dependent function, with increased endothelial permeability and increased plasma concentration of biomarkers of glycocalyx disruption (endocan), endothelial inflammation (soluble vascular cell adhesion molecule 1), vascular permeability (angiopoietin 2), and hemostasis (tissue plasminogen activator and plasminogen activator inhibitor 1), in line with the concept of vicious circle relations between impaired endothelial glycocalyx and endothelial dysfunction.

What Are the Clinical Implications?

- Given the pattern of changes of early and late manifestations of endothelial dysfunction in atherosclerosis demonstrated herein, early diagnosis of endothelial dysfunction should be focused on the assessment of the features of the impaired endothelial phenotype that display the maximal response in the early stage, while monitoring of the endothelial dysfunction progression should be based on those manifestations of endothelial dysfunction that show progressive nature along the development of disease.
- Given the complex multiparametric nature of endothelial dysfunction, therapy of endothelial dysfunction should be targeted simultaneously to multiple features but not only to single characteristics of the phenotype of dysfunctional endothelium.

cardiovascular diseases; and it has therapeutic significance (eg, in atherosclerosis,[3] hypertension,[4] heart failure,[5] and noncardiovascular diseases, such as cancer).[6]

Among various functional and biochemical features of endothelial dysfunction, impaired NO-dependent vasodilation is of particular importance in clinical studies because its measurement enables the diagnosis of malfunction of the endothelium[7] and predicts adverse cardiovascular events.[8,9] Assessment of NO-dependent vasodilation in humans is based on measurement of changes in vessel diameter in response to chemical or physical stimuli, with various detection techniques being used, including angiography,[10] plethysmography,[11] tonometry,[12] and Doppler ultrasonography.[13] In clinical settings, invasive methods are of limited use. Therefore, various

noninvasive techniques for assessing endothelium-dependent artery dilation are currently used, including 2 major approaches: flow-mediated dilation (FMD) in the brachial artery,[14,15] measured by ultrasonography, a method regarded as a gold standard; and reactive hyperemia (RH-PAT) in peripheral circulation, measured by tonometry of the finger.[16]

Magnetic resonance imaging (MRI) provides another approach for vascular wall imaging with high spatial and temporal resolution, useful for studying endothelium-dependent mechanisms of health and disease in the clinical setting.[17,18] MRI in vivo also represents a state-of-the-art technique to measure endothelial function in experimental animals.[19,20] Indeed, simultaneous assessment of endothelium-dependent vasodilation, together with quantification of endothelial permeability by MRI in vivo analysis, provides a unique insight into endothelial function in vivo.[21,22]

In gene-targeted mouse models of atherogenesis, impaired NO-mediated relaxation in ex vivo vascular preparations was repeatedly demonstrated.[23–25] It was, however, claimed that in apolipoprotein E–deficient (ApoE$^{-/-}$) mice with atherosclerosis, endothelial dysfunction occurs only at the late stage of the development of atherosclerotic plaques.[24,26] Furthermore, some authors did not confirm the presence of endothelial dysfunction in ApoE$^{-/-}$ mice.[27] In turn, we previously demonstrated that in apolipoprotein E/low-density lipoprotein receptor-deficient mice (ApoE/LDLR$^{-/-}$) mice fed a chow diet, the impairment of NO-dependent relaxation in conduit vessels of ApoE/LDLR$^{-/-}$ mice occurs before the development of atherosclerotic plaque, supporting the key role of dysfunctional endothelium in the initiation of atherogenesis in this mouse model of atherosclerosis as it is well accepted in atherosclerosis in humans.[28] However, the previous study was performed with the use of ex vivo assessment of endothelium-dependent vasodilation, not in vivo based on the MRI technique that has been recently adapted for measurement of endothelial function in vivo in mice.[20,22]

Apart from the impairment of NO-dependent function, the phenotype of dysfunctional endothelium involves a plethora of biochemical and functional changes that contribute to the pathophysiological characteristics of endothelial dysfunction, including proinflammatory mechanisms (eg adhesion molecules), prothrombotic mechanisms (eg von Willebrand factor and plasminogen activator inhibitor 1),[29] glycocalyx injury,[30] and endothelial stiffness.[31] Damage in the glycocalyx, the brushlike surface layer composed of proteoglycans and glycoproteins lining the luminal surface of the endothelium, was suggested to favor or even to trigger the development of the endothelial dysfunction.[32] In fact, release of NO is stimulated by mechanotransduction of laminar blood flow–mediated shear stress, being a main regulator of endothelial function,[33] whereas the oscillating or turbulent flow results in the proinflammatory and proatherogenic phenotype of

endothelial cells.[34] Core proteins of glycocalyx may take part in the endothelial mechanotransduction.[35] The importance of this endothelial surface in the modulation of vascular permeability,[36] the regulation of hemostasis,[37] and the progression of atherosclerosis[38–40] is also well documented.

Endothelial stiffness accompanies the loss of glycocalyx coverage and also represents an important nanomechanical feature of endothelial dysfunction,[31] but whether it precedes or follows impairment of NO-dependent function is not clear.[41–43]

To the best of our knowledge, there are no reports that have simultaneously and comprehensively analyzed the functional and biochemical phenotype of endothelium in vivo as well as the glycocalyx phenotype in an experimental murine model of atherosclerosis; and no reports have defined whether glycocalyx injury precedes the impairment of endothelium-dependent vasodilation and several other features of endothelial dysfunction or whether these events coincide. Accordingly, the aim of the present study was to characterize changes in endothelium-dependent vasodilation and endothelial permeability, NO production, various protein biomarkers of endothelial dysfunction, endothelium stiffness, and glycocalyx degradation in the early phase of atherosclerosis progression before the occurrence of atherosclerotic plaques (as verified by histological staining with Unna's orcein combined with Martius, Scarlet, and Blue trichrome [OMSB]) in comparison to the late phase of atherosclerosis with the presence of advanced plaques, in 4- to 8- and 28-week-old ApoE/LDLR$^{-/-}$ mice, respectively. The present study was performed using a 3-dimensional (3D) MRI-based method to assess endothelial function in vivo,[20,22] an atomic force microscope (AFM)–based method to detect glycocalyx degradation and endothelial stiffness,[31] a micro–liquid chromatography (microLC)/mass spectrometry (MS)–multiple reaction monitoring (MRM)–based method to assess the biomarker profile of endothelial dysfunction,[44–46] as well as an electron paramagnetic resonance (EPR)–based method to assess vascular NO production in the aorta ex vivo.[47]

Materials and Methods

The data, analytic methods, and study materials will be made available on request to other researchers for purposes of reproducing the results or replicating the procedure.

Animals

Studies were performed in female ApoE/LDLR$^{-/-}$ mice at the age of 4, 8, and 28 weeks, the model initially described by Ishibashi et al[48] and characterized by us in our previous studies.[28,49–53] In ApoE/LDLR$^{-/-}$ mice, spontaneous atherosclerosis develops without administration of an atherogenic

diet.[52] Moreover, endothelial dysfunction in this model precedes the atherosclerotic plaque development, similarly as it occurs in humans,[53] whereas the early development of endothelial dysfunction in single ApoE$^{-/-}$ mice was not univocally accepted.[24,27] Because sex determination was based solely on external inspection, not internal anatomical features, in all mice, including the group of young mice (4-week-old), although unlikely, the number of female mice in this youngest experimental group could have been lower. Young (8-week-old) control (C57BL/6) female mice, without endothelial dysfunction, were used for comparison. To verify the progression of atherosclerosis in this model, a histological assessment of size and composition of atherosclerotic plaque was performed in 8-, 10-, 18-, and 28-week-old female ApoE/LDLR$^{-/-}$ mice. ApoE/LDLR$^{-/-}$ mice, bred in the Department of Human Nutrition, University of Agriculture (Krakow, Poland), and C57BL/6 mice, bred in the Mossakowski Medical Research Centre, Polish Academy of Sciences (Warsaw, Poland), were transported to the animal house at the Institute of Nuclear Physics (Krakow, Poland) to assess endothelial phenotype in vivo. After in vivo measurements, mice were euthanized to collect blood and tissues for other measurements. The size of a given experimental group is reported in the legends of the corresponding graphs. All mice (body weight of 20–30 g) were bred in standard conditions (12 hr. light 12 hr. dark, humidity, 60%; temperature, 23°C) and housed in pathogen-free settings. All experiments were approved by the Ethics Local Committee of Jagiellonian University (Krakow, Poland) and were performed in accordance with the *Guide for the Care and Use of Laboratory Animals* of the National Academy of Sciences (National Institutes of Health publication 85-23, revised 1996), as well as the Guidelines for Animal Care and Treatment of the European Community.

Magnetic Resonance Imaging

MRI experiments were performed using a 9.4 T scanner (BioSpec 94/20 USR; Bruker, Germany). During the experiment, mice were anaesthetized using isoflurane (Aerrane; Baxter Sp. z o. o., Poland; 1.5 volume percentage) in an oxygen/air (1:2) mixture. Heart function (rhythm and ECG), respiration, and body temperature (maintained at 37°C using circulating warm water) were monitored using a Monitoring and Gating System (SA Inc, Stony Brook, NY, USA). Mice were imaged in the supine position to test endothelial function and permeability in various vessels.

Assessment of Endothelium-Dependent Vasodilation in vivo by MRI

Endothelium-dependent vascular responses in vivo were assessed by 2 techniques, as described previously,[20,22] measurements of endothelium-dependent response to acetylcholine

administration and FMD in response to reactive hyperemia, the latter considered to be a gold standard in studies on endothelial dysfunction in humans.[14,15] Response to injection of acetylcholine (Sigma-Aldrich, Poznan, Poland; 50 µL, 16.6 mg/kg,

i.p.) was analyzed in the brachiocephalic artery (BCA) and the abdominal aorta (AA), whereas FMD after short-term (5-minute) occlusion was analyzed in the femoral artery (FA), induced by a homemade vessel occlusion, as described elsewhere.[22] The
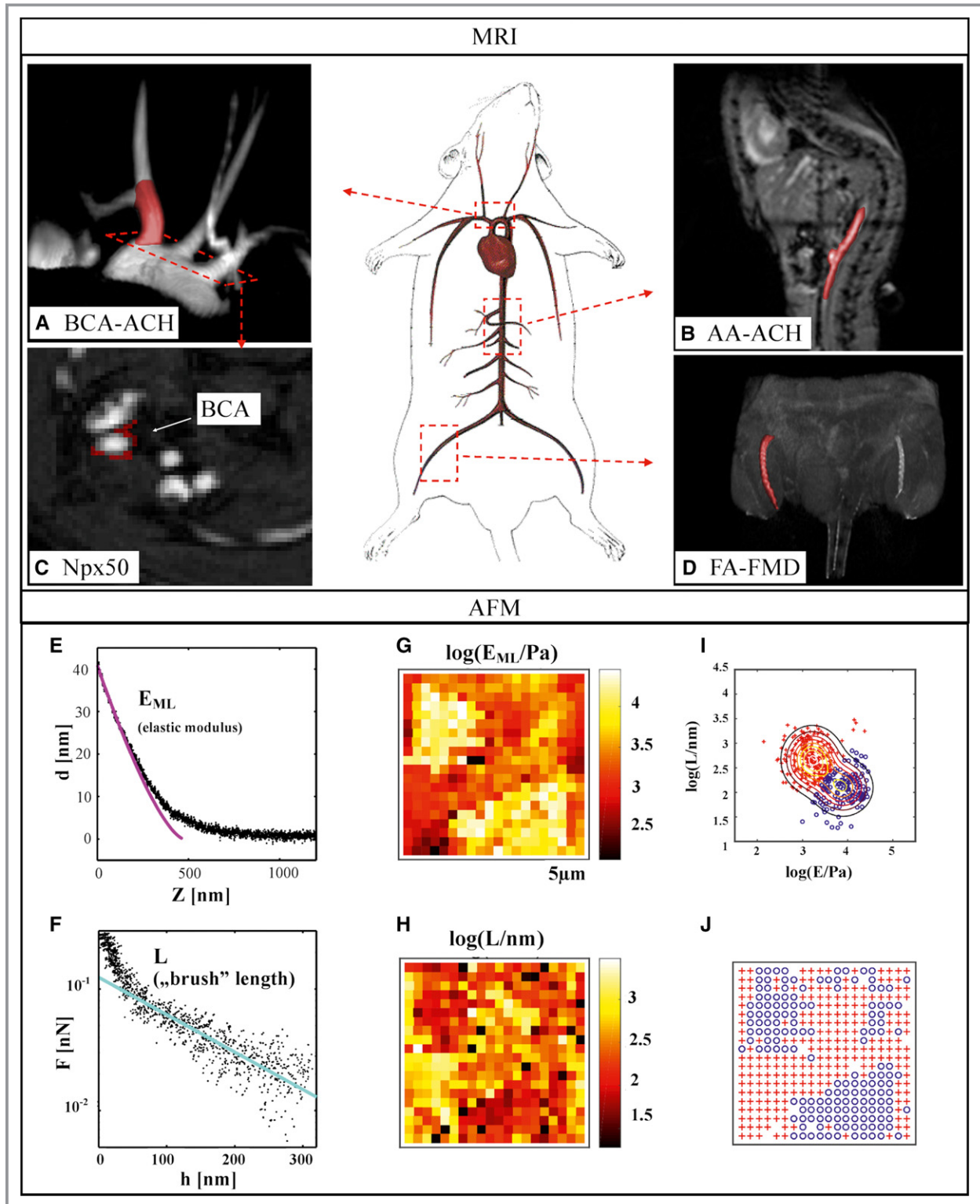
dose of acetylcholine used to assess endothelium-dependent vasodilation in vivo in mice was based on a previous study.[19] More important, endothelium-dependent response, induced by acetylcholine, as measured 25 minutes after injection, was independent of the effect of acetylcholine on the heart and respiration, as described previously.[20] Vasomotor responses were examined by comparing 2 time-resolved 3D images of the vessels before and 25 minutes after intraperitoneal acetylcholine administration or after 5 minutes of vessel occlusion. The optimal time to measure acetylcholine-induced vasorelaxation and the optimal time for vascular occlusion to measure FMD response were chosen on the basis of our previous work[20] and of other authors.[54] As reported earlier, acetylcholine-induced response in the BCA was fully blocked by N-nitro l-arginine methyl ester (L-NAME), supporting the notion that this response represents NO-dependent vasodilation.[20] Similarly, acetylcholine-induced response in the aorta and FMD in the FA were also substantially impaired by L-NAME (A. Bar; 2018, unpublished data). Images were acquired using the cine IntraGate® FLASH 3D sequence, reconstructed with the IntraGate 1.2.b.2 macro (Bruker). End-diastolic volumes of vessels were analyzed using ImageJ software 1.46r (National Institutes of Health, Bethesda, MD, USA), and scripts were written in Matlab (MathWorks, Natick, MA, USA). Imaging parameters included the following: repetition time, 6.4 ms; echo time, 1.4 ms; field of view, $30\times30\times5$ mm^3; matrix size, $256\times256\times30$; flip angle, 30°; and number of accumulations, 15 (reconstructed to 7 cardiac frames). Total scan time was 10 minutes.

Time-resolved 3D images of the aortic arch were analyzed to endothelial function assessment in BCA. Images were reconstructed to 7 cardiac frames and imported into ImageJ as a hyperstack (Figure 1A; matrix, 256×256; slices, 30; frames, 7). Further analysis was performed in the diastole of BCA, using a small hyperstack (Figure 1A, marked in red; matrix, 256×256; slices, 5; frames, 1) starting at the base of the vessel and ending just before the branch. A detailed analysis was described in the Supplementary Material of our previous work.[20] 3D images of the AA were positioned on the sagittal view of the mice, ≈5 mm under the heart (Figure 1B). Analysis was performed in the diastole of the AA in ImageJ using a small hyperstack (Figure 1B, marked in red; matrix, 256×256; slices, 10; frames, 1). 3D images of the FA were positioned on coronal view of the mice, on the right hind limb of the mouse. Analysis was performed in ImageJ using a small hyperstack (Figure 1D, marked in red; matrix, 256×256; slices, 7; frames, 1). All cross-sectional areas of vessels at each slice were obtained using thresholding segmentation and exported to Matlab, where vessel volumes were reconstructed and calculated.

Assessment of Endothelial Permeability in vivo by MRI

Measurements of endothelial permeability were performed using a unique formulation of gadolinium contained in the liposome (gadodiamide in the liposome, concentration of formulation: 287 mg/mL, 4.5 mL/kg, *i.v.*). The liposomal formulation of gadolinium was prepared according to the original method[55]; in short, highly purified phosphatidylcholine (Lipoid, Germany), dissolved in propylene glycol, was mixed with buffered aqueous solution containing an appropriate amount of gadolinium and was followed by force-controlled extrusion, producing a uniform liposome suspension (medium size of 110 ± 6 nm; polydispersity index, 0.1). The proportion of liposome-forming components was 30:20:50 w/w/w of the lipid/glycol/aqueous phase. The size distribution of resulting liposomes was measured using the dynamic light scattering method (Zetasizer NanoZS, Malvern, UK). The concentration of gadolinium was

Figure 1. Method for magnetic resonance imaging (MRI)–based in vivo assessment of endothelial function and permeability (**A** through **D**) as well as method of analysis and classification of nanoindentation data (**E** through **J**). MRI-based assessment of endothelium-dependent response to acetylcholine administration, expressed as changes in vessel volume, was performed in the brachiocephalic artery (BCA) visible on the 3-dimensional (3D) image of the aortic arch (**A**) and in the abdominal aorta (AA) positioned on the sagittal view of the mouse (**B**). **C**, Endothelial permeability changes were assessed on the basis of number of pixels, for which relaxation time had changed >50% after contrast agent administration (Npx50); representative image of vessel cross-sections, with pixels taken for analysis, is marked in red. **D**, Flow-mediated endothelium-dependent dilation (FMD), also expressed as changes in the vessel volume, was assessed in the femoral artery (FA), visible on the 3D image of the right hind limb of the mouse. **E**, Atomic force microscope (AFM)–based raw indentation curve d(Z) is shown. The solid magenta line shows a curve fitted using the Hertz model in the region of maximum load for which one can assume that the brush is squeezed. From the Hertz fit, the values of endothelium elastic modulus (E_{ML}) were extracted. Brush length (L) was calculated from the exponential part of the force-separation curve F(h), according to the model of Alexander–de Gennes. **F**, The solid cyan line shows the fitted model in the region of lower indentations. **G**, An example of the apparent E_{ML} map created from a set of 20×20 indentation curves d(Z) is shown. **H**, A corresponding map, which shows the spatial distribution of L, is shown. **I**, Scatter plots representing values of apparent E_{ML} and L. Gaussian mixture distributions with 2 components were fitted to the data to differentiate areas with (red) and without (blue) glycocalyx coverage. **J**, Spatial maps of glycocalyx distribution. Data points shown using red crosses and blue circles are classified on the basis of an automatic clustering procedure and represent regions with and without glycocalyx, respectively.

determined by steady-state fluorescence of the compound at an emission wavelength of 310.5 nm after excitation at 275 nm (Fluoromax 4; TCSPC Horiba Jobin Yvon). The encapsulation efficiency of gadolinium after extrusion was $77\pm5\%$. The excess of the contrast agent in the final formulation was removed using the ultrafiltration method (Amicon Ultra, 10 kDa).

To assess permeability in the BCA, relaxation time (T_1) maps were measured before and 30 minutes after intravenous administration of gadolinium-rich liposome contrast agent (gadolinium-liposome) using the variable flip angle technique,[56,57] by sampling the signal, using varying values of flip angles and then fitting the result to an expected T_1-dependent signal model, as described previously.[20,58] 3D images of the aortic arch were acquired using the 3D IG-FLASH sequence, to obtain high transmit (B_1) magnetic field profile uniformity within measured subslices. Imaging parameters included the following: repetition time, 10 ms; echo time, 1.1 ms; field of view, $30\times30\times4$ mm^3; matrix size, $192\times160\times8$; number of repetitions, 12; and cardiac frames, 1. Eight flip angles were used: $2°$, $4°$, $6°$, $8°$, $14°$, $20°$, $30°$, and $50°$. Flip angle values were set by changing the length of an radio frequency pulse, with constant amplifier power. The total scan time for all angles was 16 minutes.

Obtained images were used to calculate the T_1 around the BCA lumen before and after gadolinium-liposome administration. The signal model was fitted pixel by pixel using Matlab software, developed in house. Two T_1 maps (before and after contrast agent administration) were compared, using scripts written in Matlab, and pixels for which T_1 had changed significantly (by >50%) after gadolinium-liposome administration were marked in red (Figure 1C). The threshold value (50%) was determined experimentally. All red pixels were counted by the program as the number of pixels for which T_1 had changed by >50% (Npx50) after gadolinium-liposome administration.

Blood Sampling and Biochemical Analysis

After in vivo measurements, ApoE/LDLR$^{-/-}$ mice were anesthetized (100 mg/kg ketamine+10 mg/kg xylazine, *i.p.*) and blood was drawn from the heart and collected in tubes containing EDTA (10% solution of dipotassium EDTA; Aqua-Med, Łodz, Poland; 1 μL of EDTA/100 μL of blood). Next, blood was mixed with MS-SAFE Protease and Phosphatase Inhibitor (Sigma-Aldrich, Poznan, Poland) in a ratio of 100:1. All samples were centrifuged at $664g$, at a temperature of $4°C$ for 10 minutes to isolate plasma. Obtained plasma samples were deep frozen at $-80°C$ for measurements of biomarkers of endothelial dysfunction (50 μL). The Aorta and the BCA were collected for further ex vivo assessments, as described below.

Assessment of Glycocalyx Coverage and Length by AFM

The aorta samples were resected from the abdominal fragment of the aorta. To prepare en face samples of aortas, a protocol described by Targosz-Korecka et al[31] was used. After harvesting and cleaning, the aorta was cut into small patches to expose the inner wall of the aorta. The patches of the aorta were gently transferred onto a glass coverslip coated with Cell-Tak (BD Biosciences, Bedford, MA USA). Each patch of the aorta was glued to the glass, leaving the endothelial surface facing upward. After preparation, the samples were placed in Hanks' balanced salt solution buffer, supplemented with 1% fetal bovine serum, 1% penicillin/streptomycin, and 5 mmol/L glucose, and were left to equilibrate for 1 hour. The AFM nanoindentation experiment was performed within 2 to 3 hours after the isolation.

Acquisition of AFM Indentation Curves

AFM nanoindentation experiments were performed with a NanoWizard III system (JPK, Germany). All measurements were performed on unfixed aorta samples immersed in Hanks' balanced salt solution supplemented with 1% fetal bovine serum, 1% penicillin/streptomycin, and 5 mmol/L glucose. A spherical colloidal probe with a nominal diameter of 4.5 μm, attached to a cantilever (NovaScan, USA), with a spring constant of 0.01 N/m, was used in experiments. The indentation curves were recorded for a maximal loading force of 1 nN at a velocity of 1.5 μm/s. For each aorta sample, spatial maps of indentation curves were recorded at many random positions of the sample. Typically, each region of interest comprised 10×10 curves that were recorded on a 20×20 μm grid.

Analysis and Classification of Indentation Curves

Calculation of nanomechanical parameters of the endothelium from mouse AA was performed on the basis of the analysis and classification methods described previously by Targosz-Korecka et al.[31] The mean nanomechanical parameters of glycocalyx (brush length [L] and glycocalyx coverage [N]) and endothelium (elastic modulus [E_{ML}]) were calculated in a 2-step procedure. In the first step, based on the method proposed by Sokolov et al,[59] the Hertz model was fitted to the indentation curves in the region of maximum load and the values of cell E_{ML} were extracted (Figure 1E). Next, for lower indentations, a force curve based on Alexander–de Gennes' theory of polymer brushes was fitted for description of glycocalyx properties (glycocalyx length; Figure 1F). Based on calculated parameters, the spatial maps were performed, as presented in Figure 1G and 1H. In the second step,

classification of curves based on the clustering methods was performed to distinguish between curves with and without the glycocalyx part. This procedure is based on a classification scheme that uses 2 independent parameters, E_{ML} and brush length, as proposed by Targosz-Korecka et al.[31] Because of a large spread in the values, these parameters were transformed to a logarithmic E_{ML}–brush length scale and displayed on scatter plots. A bivariate gaussian mixture was fitted to the data points using Matlab. Next, a clustering procedure was used to assign data into the specific component of the gaussian mixture distribution with the criterion of the largest posterior probability for the observation, weighted by the component probability. As a result, all indentation curves were classified as recorded on regions without glycocalyx and regions with glycocalyx (Figure 1I and 1J).

Assessment of Endothelial NO Production in Aorta Using EPR

For measurements of endothelial NO synthase–dependent NO production, EPR spin trapping with diethyldithiocarbamic acid sodium salt was used ex vivo, as described previously,[47] with minor modifications. Isolated aorta was cleared from surrounding tissue, opened longitudinally, and preincubated with 10 μmol/L N6-(1-iminoethyl)-lysine, hydrochloride in Krebs-HEPES buffer for 30 minutes at 37°C in a well of a 48-well plate. Addition of N6-(1-iminoethyl)-lysine, hydrochloride during the preincubation period allowed the direct measurements of NO produced by endothelial NO synthase without the signal from NO produced by inducible NO synthase, expressed by macrophages in atherosclerotic plaque.[60] Next, diethyldithiocarbamic acid sodium salt (3.6 mg) and FeS-O_4·7H_2O (2.25 mg) were separately dissolved under argon gas bubbling in two 10-mL volumes of ice-cold Krebs-HEPES buffer and were kept under gas flow on ice until used. After preincubation, a spin trap (125 μL of FeSO$_4$·7H_2O and 125 μL of diethyldithiocarbamic acid sodium salt; final concentration of the colloid, 285 μmol/L) and calcium ionophore A23187 (final concentration, 1 μmol/L) were added to the aorta. Subsequently, incubation for 90 minutes at 37°C was started. To detect NO release, calcium ionophore, but not acetylcholine, was used to provide receptor-independent, prolonged stimulation of NO production during incubation, as acetylcholine-induced receptor-dependent transient activation of NO release was insufficient for EPR-based detection. Finally, dried aorta was weighed and frozen in liquid nitrogen (suspended in fresh buffer) into the middle of a 400-μL column of Krebs-HEPES buffer and stored at −80°C until measured. EPR spectra were obtained using an X-band EPR spectrometer (EMX Plus; Bruker, Germany), equipped with a rectangular resonator cavity H102. Signals

were quantified by measuring the total amplitude of the Fe(II)-Diethyldithiocarbamate after correction of baseline. The quantitative results of NO production, assessed by EPR, were expressed in arbitrary units/mg of tissue.

Assessment of Biomarkers of Endothelial Dysfunction in Plasma by MicroLC/MS-MRM

Assessment of 10 protein biomarkers of endothelial dysfunction was performed using the microLC/MS-MRM method. The panel included biomarkers of various aspects of endothelial dysfunction, such as the following: glycocalyx disruption: syndecan-1 (SDC-1) and endocan (ESM-1); endothelial inflammation: soluble vascular cell adhesion molecule 1 (sVCAM-1), the soluble form of E-selectin (sE-sel) and soluble intercellular adhesion molecule 1 (sICAM-1); endothelial permeability: angiopoietin 2 (Angpt-2) and the soluble form of fms-like tyrosine kinase (sFLT-1); and hemostasis: von Willebrand factor (vWF), tissue plasminogen activator (t-PA), and plasminogen activator inhibitor 1 (PAI-1).

The Nexera ultra-high performance liquid chromatography (UHPLC) system (Shimadzu, Kyoto, Japan) connected with a highly sensitive mass spectrometer QTrap 5500 (Sciex, Framingham, MA, USA) were used. During sample preparation, the studied mouse material was subjected to proteolytic digestion using porcine trypsin to achieve unique and reproducible peptide sequences, applied as the surrogates of the proteins suitable for LC-MS/MS analyses. A detailed description of the targeted analysis focused on the panel of selected proteins was presented elsewhere.[44–46]

Histological Assessment of Atherosclerotic Plaque

For determination of the atherosclerotic plaque area and composition, isolated BCA was dissected, fixed in 4% buffered formalin, and embedded in paraffin. Serial sections of the BCA (5-μm thick) were collected from the proximal to distal part of the artery. Our originally developed staining with OMSB, as described recently by us elsewhere,[61] was applied on every tenth section of cross-sectional slices (50 μm interval between each section) for visualization of collagen, elastin, fibrin, red blood cells, and vascular smooth muscle cells within the atherosclerotic plaque. The areas of particular components of atherosclerotic plaque as well as artery lumen and vascular wall area were determined after Columbus-based software processing using an algorithm previously developed by our group.[61] The parameters analyzed include vessel wall area, internal vessel area (IVA), plaque area (expressed as percentage of IVA: plaque/IVA), lumen area (expressed as percentage of IVA: lumen/IVA), as well as areas of collagen and lipids in plaque (collagen/plaque and lipid/plaque, respectively).

Statistical Analysis

Obtained data are presented as mean and SD or, in case of the lack of normal distribution, as median and interquartile range. Statistical tests were performed using STATISTICA 10 (Stat Soft Inc, USA). Nonparametric (Kruskal-Wallis test) or parametric (1-way ANOVA with an honestly significant difference Tukey's test for unequal sample sizes) tests were performed. $P=0.05$ was considered to be statistically significant.

Results

Changes in Acetylcholine-Induced Vasodilation and Flow-Mediated Vasodilation in vivo in ApoE/LDLR$^{-/-}$ Mice

In the AA (Figure 2A), even in 4-week-old ApoE/LDLR$^{-/-}$ mice, acetylcholine-induced vasodilation was impaired (volume changes, ≈23%) compared with control mice (volume changes, ≈33%); in 8-week-old ApoE/LDLR$^{-/-}$ mice,
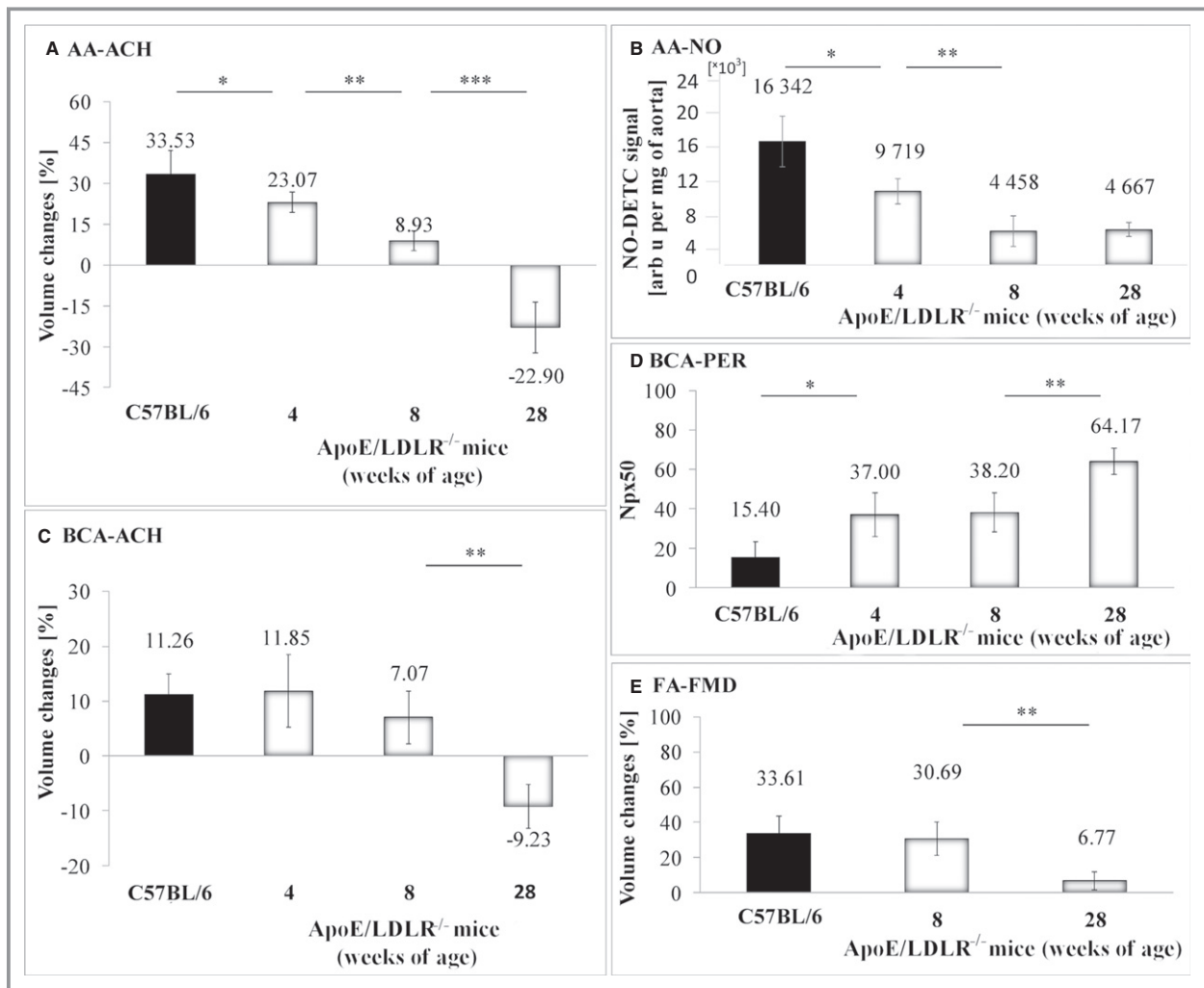

Figure 2. Progression of the impairment of endothelium-dependent vasodilation, vascular NO production, and increased endothelial permeability in apolipoprotein E/low-density lipoprotein receptor-deficient mice (ApoE/LDLR$^{-/-}$) mice. Changes in end-diastolic volume of the abdominal aorta (AA-acetylcholine [ACH]; **A**) and the brachiocephalic artery (BCA-acetylcholine [ACH]; **C**) 25 minutes after acetylcholine administration; changes in NO production in the aorta, measured by spin trapping with diethyldithiocarbamic acid sodium salt (DETC) (AA-NO; **B**); changes in endothelial permeability described as Npx50 value, which represents the number of pixels around the BCA lumen, for which relaxation time had changed >50% (Npx50) after injection of gadolinium-rich liposome contrast agent (BCA-permeability [PER]; **D**); and changes in volume of the femoral artery (FA–flow-mediated dilation [FMD]; **E**) after 5-minute vessel occlusion in ApoE/LDLR$^{-/-}$ mice (white columns) at the age of 4 (n=4 for **A**, **C**, and **D**; and n=7 for **B**), 8 (n=6 for **A**, **B**, **C**, and **E**; and n=5 for **D**), and 28 (n=4 for **A**, n=8 for **B**, n=7 for **C**, n=6 for **D**, and n=5 for **E**) weeks in comparison to 8-week-old control, C57BL/6 mice (n=4 for **A**, n=6 for **B**, n=7 for **C**, and n=5 for **D** and **E**; black columns). Statistics: bootstrap-boosted estimate of 1-way ANOVA, followed by Tukey's post hoc test (**A**, **C**, and **D**), and ANOVA, followed by Tukey's post hoc test (**B** and **E**) (normality was assessed using Shapiro-Wilk test). *P<0.05, **P<0.01, ***P<0.001.

acetylcholine response was further impaired (volume changes, ≈9%); while in 28-week-old ApoE/LDLR$^{-/-}$ mice, acetylcholine response changed to vasoconstriction (volume changes, ≈−23%). At the early stage of endothelial dysfunction in 4- to 8-week-old ApoE/LDLR$^{-/-}$ mice, stimulated NO production (Figure 2B) in the AA was reduced by ≈41% and 73% in 4- and 8-week-old mice, respectively, compared with control mice. Interestingly, stimulated vascular NO production in the aorta was not further impaired in older animals, and was similar in 8- and 28-week-old ApoE/LDLR$^{-/-}$ mice. In the BCA (Figure 2C), there was also a tendency for the early impairment of acetylcholine-induced vasodilation, but these changes were not significant in 4- to 8-week-old ApoE/LDLR$^{-/-}$ mice (volume changes, ≈10%). Similar to the AA, in the BCA, acetylcholine response also led to vasoconstriction (volume changes, ≈−9%) in 28-week-old ApoE/LDLR$^{-/-}$ mice. In contrast to acetylcholine-induced vasodilation, flow-mediated

vasodilation (Figure 2E) was fully preserved in the FA in 8-week-old ApoE/LDLR$^{-/-}$ mice (volume changes, ≈30%) but was impaired in 28-week-old ApoE/LDLR$^{-/-}$ mice (volume changes, ≈7%).

Changes in Endothelial Permeability in ApoE/LDLR$^{-/-}$ Mice in vivo

In 4- to 8-week-old ApoE/LDLR$^{-/-}$ mice, endothelial permeability was increased. As shown in Figure 2D, there was a significant increase in the Npx50 parameter of the T_1 signal around the BCA lumen (increase by ≈140% and 148% for 4- and 8-week-old mice, respectively, in comparison to control) after intravenous injection of gadolinium-containing liposomes. In 28-week-old ApoE/LDLR$^{-/-}$ mice, the increase in endothelial permeability was more pronounced compared with 4- to 8-week-old ApoE/LDLR$^{-/-}$ mice.
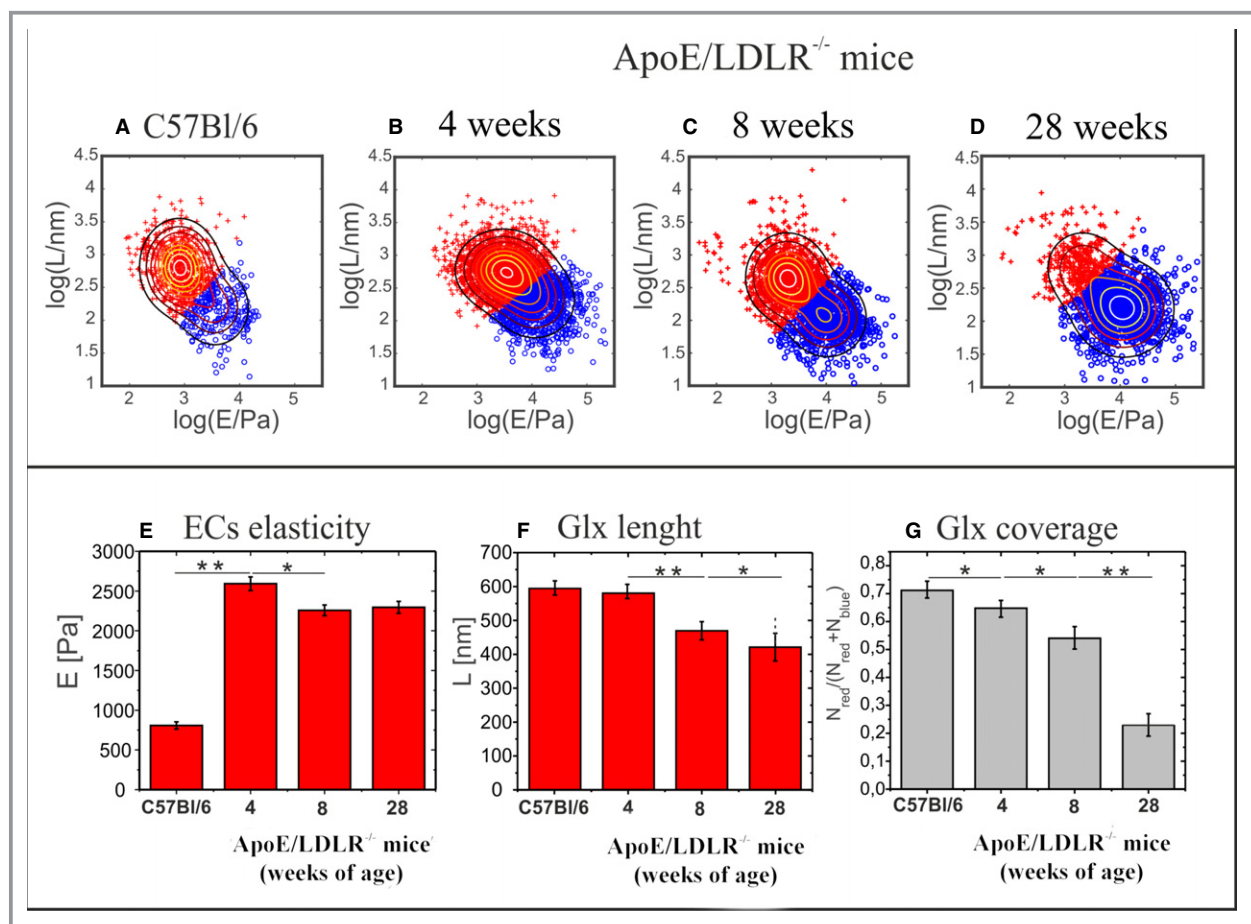

Figure 3. Distinction of nanoindentation data measured on glycocalyx (Glx) layer as well as endothelium stiffening and glycocalyx degradation in abdominal aorta from apolipoprotein E/low-density lipoprotein receptor-deficient mice (ApoE/LDLR$^{-/-}$). Total atomic force microscope nanoindentation data set and its classification shown in the form of scatter plot of the elastic modulus vs brush length (L). Data points shown in red (endothelium with glycocalyx) and blue (endothelium without glycocalyx) were classified using an automatic clustering procedure: C57Bl/6 mice (**A**) and ApoE/LDLR$^{-/-}$ mice at the ages of 4 (**B**), 8 (**C**), and 28 (**D**) weeks (n=4 for each group). **E**, Elastic modulus (E) of the endothelium (ECs elasticity indicates elasticity of endothelial cells). **F**, Glycocalyx length. **G**, Glycocalyx coverage. Statistical significance was tested by 1-way ANOVA, followed by Tukey's post hoc test. *$P<0.05$, **$P<0.01$, ***$P<0.001$.

Biomarkers of glycocalyx disruption (SDC-1, ESM-1)

A — SDC-1 [pmol/mL]: C57BL/6 26.97; 4: 35.55; 8: 39.02; 28: 52.77 (**)

B — ESM-1 [nmol/mL]: C57BL/6 0.0076; 4: 0.0105; 8: 0.0093; 28: 0.0085 (**)

Biomarkers of endothelial permeability (sFLT-1, Angpt-2)

F — sFLT-1 [nmol/mL]: C57BL/6 0.22; 4: 0.25; 8: 0.22; 28: 0.40 (***)

G — Angpt-2 [nmol/mL]: C57BL/6 0.52; 4: 1.48; 8: 1.05; 28: 1.49 (***, ***)

Biomarkers of endothelial inflammation (sVCAM-1, sICAM-1, sE-sel)

C — sVCAM-1 [pmol/mL]: C57BL/6 18.62; 4: 31.55; 8: 30.74; 28: 22.51 (*, *)

D — sICAM-1 [pmol/mL]: C57BL/6 2 478; 4: 2 153; 8: 3 242; 28: 1412

E — sE-sel [nmol/mL]: C57BL/6 0.27; 4: 0.22; 8: 0.24; 28: 0.18 (**)

Biomarkers of hemostasis (vWF, t-PA, PAI-1)

H — vWF [nmol/mL]: C57BL/6 5.47; 4: 6.12; 8: 4.27; 28: 4.56

I — t-PA [nmol/mL]: C57BL/6 0.75; 4: 1.13; 8: 1.14; 28: 1.40 (**, ***, ***)

J — PAI-1 [nmol/mL]: C57BL/6 0.86; 4: 1.29; 8: 1.11; 28: 1.22 (***, ***)

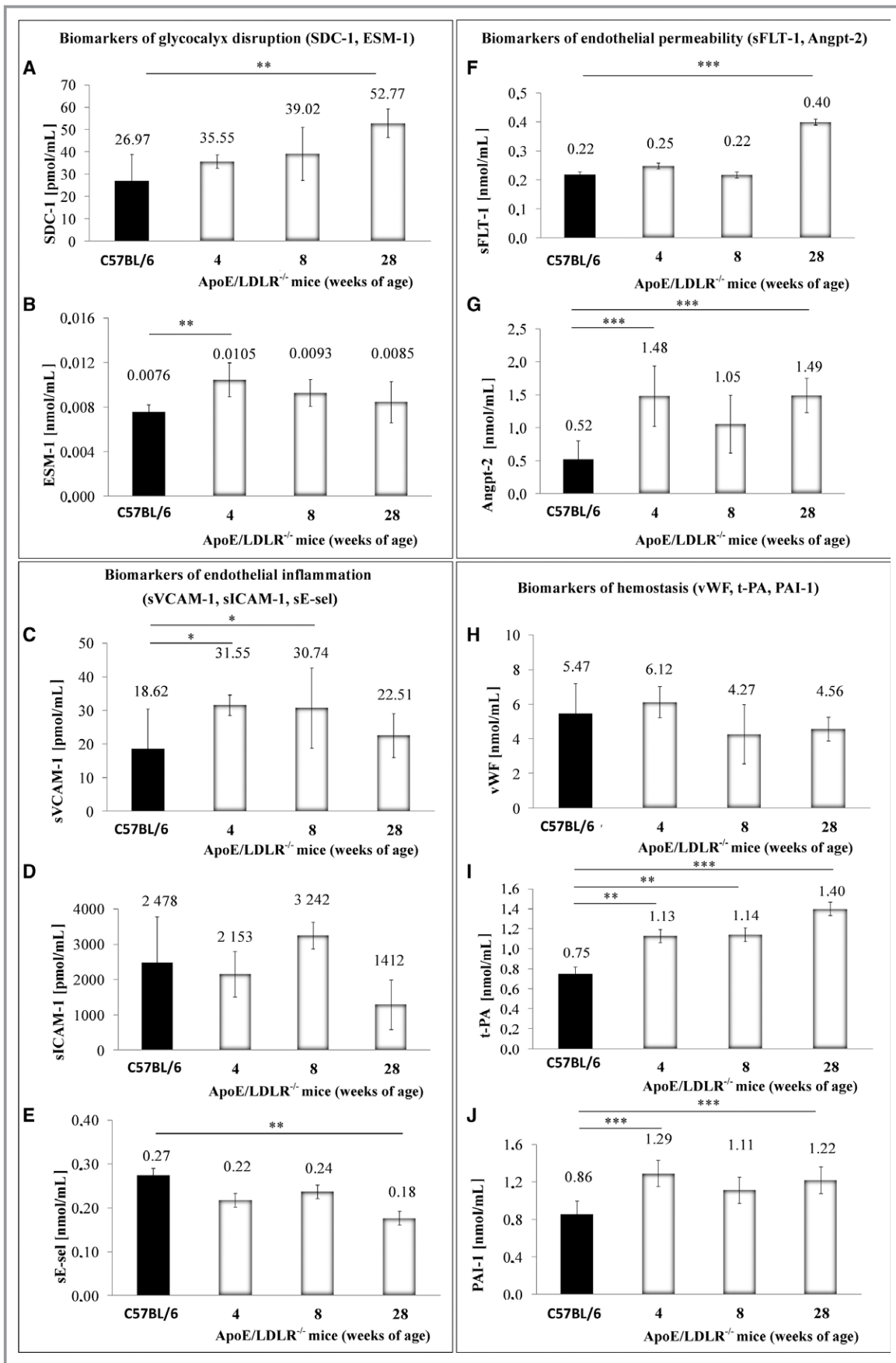ApoE/LDLR$^{-/-}$ mice (weeks of age)

Figure 4. Plasma concentration of protein biomarkers of endothelial dysfunction. Concentration of syndecan-1 (SDC-1; **A**), endocan (ESM-1; **B**), soluble vascular cell adhesion molecule 1 (sVCAM-1; **C**), soluble intercellular adhesion molecule 1 (sICAM-1; **D**), soluble form of E-selectin (sE-sel; **E**), soluble form of fms-like tyrosine kinase (sFLT-1; **F**), angiopoietin 2 (Angpt-2; **G**), von Willebrand factor (vWF; **H**), tissue plasminogen activator (t-PA; **I**), and plasminogen activator inhibitor 1 (PAI-1; **J**) in plasma, in apolipoprotein E/low-density lipoprotein receptor-deficient mice (ApoE/LDLR$^{-/-}$) mice (white columns), at the ages of 4 (n=7), 8 (n=5), and 28 (n=9) weeks in comparison to 8-week-old control, C57BL/6 mice (n=7; black columns). Statistics: 1-way ANOVA, followed by Tukey's post hoc test (**A**, **B**, **D**, and **F-J**), or the Kruskal-Wallis test, followed by Dunn's post hoc test (**C** and **E**) (normality was assessed using the Shapiro-Wilk test). *$P<0.05$, **$P<0.01$, ***$P<0.001$.

Changes in Nanomechanical Properties of Glycocalyx and Endothelium in ex vivo Aorta in ApoE/LDLR$^{-/-}$ Mice

In 4-week-old ApoE/LDLR$^{-/-}$ mice, the E_{ML} describing endothelial stiffness increased ≈3-fold and remained significantly elevated in 8- and 28-week-old ApoE/LDLR$^{-/-}$ mice. Glycocalyx coverage, but not length, was significantly reduced in 4-week-old ApoE/LDLR$^{-/-}$ mice, whereas in 8-week-old ApoE/LDLR$^{-/-}$ mice, both parameters (glycocalyx coverage and length) were significantly reduced compared with control mice. In 28-week-old ApoE/LDLR$^{-/-}$ mice, glycocalyx coverage was substantially decreased compared with 8-week-old ApoE/LDLR$^{-/-}$ mice, whereas glycocalyx length was only slightly reduced. Figure 3 shows the entire experimental data set in the form of scatter plots for the aorta taken from ApoE/LDLR$^{-/-}$ mice at the age of 4 (Figure 3B), 8 (Figure 3C), and 28 (Figure 3D) weeks compared with control C57BL/6 mice (Figure 3A). The red data points correspond to the indentation curve classified as those measured on endothelium covered by glycocalyx, whereas the blue data points represent the indentation curve for endothelium without glycocalyx. Figure 3 presents the results for measurements of E_{ML} of the endothelium (Figure 3E), glycocalyx length (Figure 3F), and glycocalyx coverage (Figure 3G) for ApoE/LDLR$^{-/-}$ mice at the ages of 4, 8, and 28 weeks compared with control mice. The mean values of the E_{ML} (Figure 3E) and the glycocalyx brush length (Figure 3F) were derived solely from indentation curves classified as "red" curves with a glycocalyx part. The glycocalyx coverage (Figure 3G) was calculated as the ratio of the number of red curves/the number of all curves measured for a given sample. The details of the AFM-based analysis are presented in Figure S1.

Changes in Plasma Concentration of Biomarkers of Glycocalyx Disruption (SDC-1 and ESM-1), Endothelial Inflammation (sVCAM-1, sICAM-1, and sE-sel), Endothelial Permeability (sFLT-1 and Angpt-2), and Hemostasis (vWF, tPA, and PAI-1) in ApoE/LDLR$^{-/-}$ Mice

In 4-week-old ApoE/LDLR$^{-/-}$ mice, the plasma concentration of the number of biomarkers significantly increased, including

at least 1 biomarker from each category: glycocalyx injury (ESM-1, increased by ≈38% in comparison to control mice) (Figure 4B), endothelial permeability (Angpt-2, increased ≈3-fold in comparison to control group) (Figure 4G), endothelial inflammation (sVCAM-1, increased by ≈70% in comparison to control mice) (Figure 4C), and hemostasis (t-PA [Figure 4I] and PAI-1 [Figure 4J], both increased by ≈1.5-fold in comparison to control group). Most of them remained elevated in 8-week-old ApoE/LDLR$^{-/-}$ mice. With the exception of SDC-1 (Figure 4A) and the sFLT-1 (Figure 4F), there was no substantial increase in plasma concentration of any of the selected biomarkers (Figure 4 D,E,H) in 28- versus 4- to 8-week-old ApoE/LDLR$^{-/-}$ mice.

Progression of Atherosclerosis in ApoE/LDLR$^{-/-}$ Mice

To confirm the absence of atherosclerotic plaques in young ApoE/LDLR$^{-/-}$ mice and the presence of advanced atherosclerotic plaques in older ApoE/LDLR$^{-/-}$ mice, OSMB histological staining was used (Figure 5A). As shown in Figure 5D–E, in 8-week-old ApoE/LDLR$^{-/-}$ mice, atherosclerotic plaques were not present. Furthermore, in 10-week-old ApoE/LDLR$^{-/-}$ mice, plaques were virtually absent. In older mice, such as 18-week-old mice, advanced forms of atherosclerotic plaque were observed, with further progression for 28-week-old mice (plaque/IVA, ≈30% and 55%, respectively). Other analyzed parameters also indicated significant progression of atherosclerosis from 18- to 28-week-old mice, including lumen narrowing, IVA (Figure 5C), and collagen content (Figure 5F) but not lipid content (Figure 5G), which was similar in 18- and 28-week-old mice groups. Atherosclerotic plaque in 18-week-old ApoE/LDLR$^{-/-}$ mice was characterized by high lipid content (lipid/plaque, ≈25%) and an almost complete lack of collagen (collagen/plaque, 0.32%), which significantly increased in 28-week-old mice (collagen/plaque, ≈9%). Despite the fact that in 8-week-old ApoE/LDLR$^{-/-}$ mice, well-defined atherosclerotic plaques were absent, in 4 of 6 mice, the vessel wall (vessel wall area, VWA, Figure 5B) of the BCA was locally thickened (70.60 versus 49.61 μm) (Figure S2A through S2C) and displayed altered vascular smooth muscle morphological features (signs of hyperplasia, hypertrophy, and extracellular matrix deposition
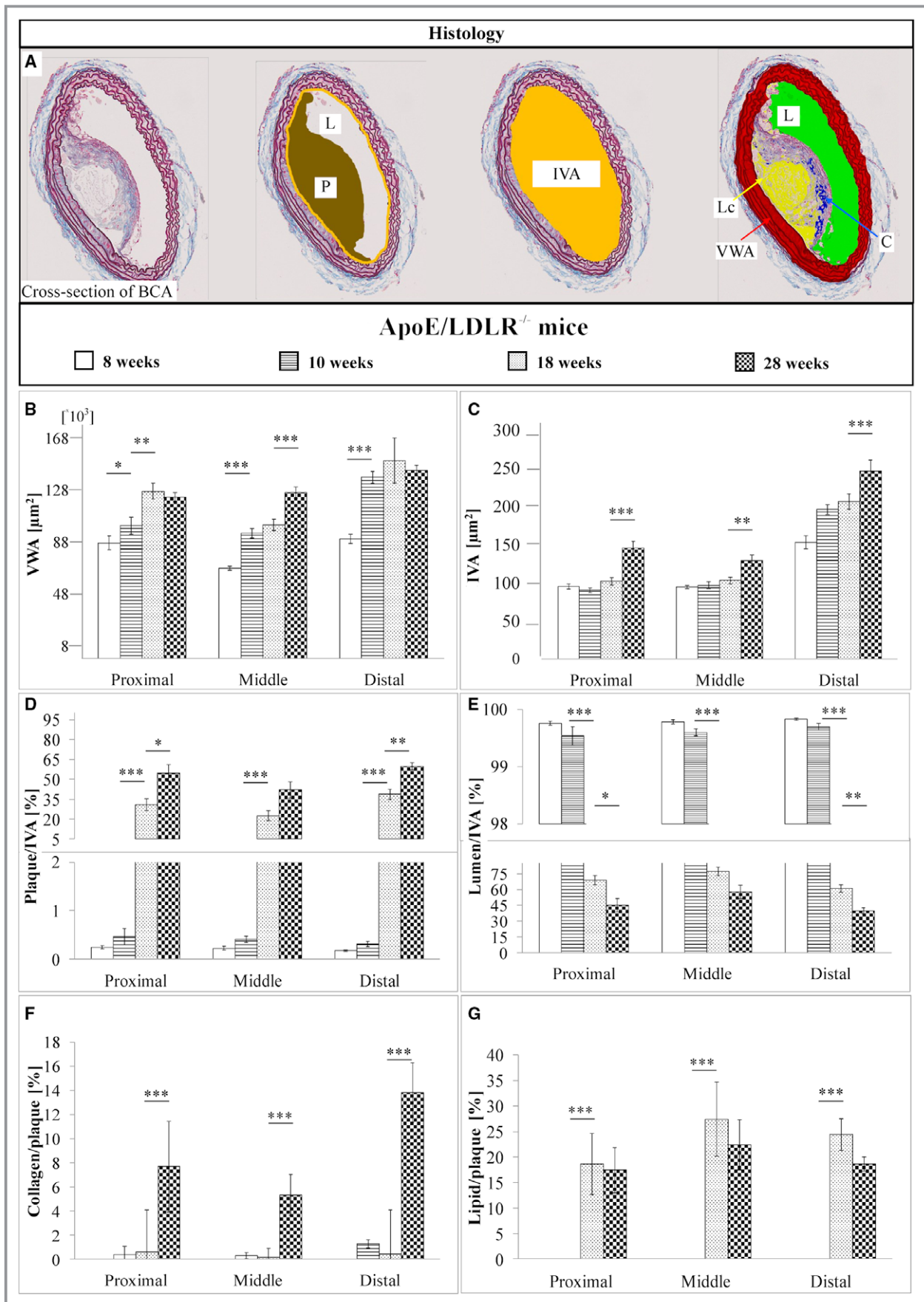
Figure 5. Atherosclerotic plaque size and composition in apolipoprotein E/low-density lipoprotein receptor-deficient mice (ApoE/LDLR$^{-/-}$) mice. **A**, Representative images of brachiocephalic artery (BCA) cross-sections stained with Unna's orcein combined with Martius, Scarlet, and Blue trichrome (OMSB), with particular components of atherosclerotic plaque (P), including lipid core (Lc), collagen, artery lumen (L), and vessel wall area (VWA), that were quantitatively determined by Columbus-based software processing. Internal vessel area (IVA) was determined as the sum of both plaque and lumen areas. Changes in vessel wall area (VWA) (**B**), IVA (**C**), plaque area (expressed as percentage of IVA: plaque/IVA; **D**), lumen area (expressed as percentage of IVA: lumen/IVA; **E**), as well as areas of collagen and lipids in plaque (collagen/plaque [**F**] and lipid/plaque [**G**], respectively) in ApoE/LDLR$^{-/-}$ mice at the ages of 8 (n=6), 10 (n=8), 18 (n=9), and 28 (n=8) weeks. The assessment was performed for divided vessel in proximal, middle, and distal parts. Statistics: Kruskal-Wallis 1-way ANOVA (normality was assessed using the Shapiro-Wilk test). *$P<0.05$, **$P<0.01$, ***$P<0.001$.

of collagen and elastin [Figure S2E], as well as a proliferative phenotype featured by a pale staining). The distance between elastic laminae and the subendothelial layer was enlarged, with evidence of smooth muscle cells migrating into the intima (Figure S2B) and monocyte adhesion (Figure S2D) and migration into the subendothelial space.

Discussion

In the present work, we comprehensively assessed the endothelial phenotype in ApoE/LDLR$^{-/-}$ mice and demonstrated that endothelial dysfunction, even at the early stage (ie prior to the development of well-defined atherosclerotic plaque), is a complex multifactorial response involving diminished glycocalyx coverage and lengths and endothelial stiffness. These factors coincide with the impairment of endothelium-dependent vasodilation, increased endothelial permeability, diminished vascular NO production, and increased plasma concentration of biomarkers of glycocalyx disruption (ESM-1), endothelial inflammation (sVCAM-1), vascular permeability (Angpt-2), and hemostasis (PAI-1 and t-PA). These results suggest that glycocalyx injury does not proceed other features of endothelial dysfunction,[62] but rather coincides with these pathogenetic endothelial events, in line with the concept of vicious circle relations between impaired endothelial glycocalyx and endothelial dysfunction.[63]

In the present work, we adopted a panel of state-of-the-art, well-suited, sensitive, and validated previously developed methods to measure endothelial function in vivo (MRI),[20] glycocalyx coverage and length (AFM),[31] concentration of multiple biomarkers of endothelial dysfunction in plasma (microLC/MS-MRM),[44–46] and vascular NO production (EPR).[47]

For the assessment of endothelial phenotype in mice in vivo, we used an MRI-based approach. Despite this method being associated with several technical challenges[64] (see review by Bar et al for details[58]), it has been found to be well suited for detection and quantification, with good sensitivity and reproducibility, of NO-dependent artery dilation in healthy mice and impaired vasodilation or artery constriction in mice exposed to a proatherogenic stimulus (eg high-fat diet) or in

mice with atherosclerosis (eg ApoE/LDLR$^{-/-}$ mice).[19–22] Undoubtedly, the important advantage of our approach to MRI-based assessment of endothelial function is a retrospective reconstruction of images from 3D data sets, allowing for analysis of changes in vessel volume instead of changes in cross-sectional vessel area only, increasing measurement accuracy.[20] Furthermore, in the present work, MRI-based assessment of endothelium-dependent vasodilation was performed in 3 arteries: in the BCA and the AA in response to intraperitoneal administration of acetylcholine and in the FA in response to flow (FMD). Vasoactive responses to acetylcholine, given the low dose in vivo in mice, are independent of the effect of acetylcholine on the heart and respiration, as shown previously;[20] thus, they can be used to reliably assess endothelial status in vivo. In turn, FMD was a similar assay of endothelial function in vivo in mice as that used in humans in the brachial artery and was described in detail in supplementary material in our previous study.[22] Noteworthy, to date, there are only a few reports describing evaluation of FMD using ultrasonography[65,66] or optical tomography of the coherence[54,67] in small experimental animals. In our hands, the MRI-based method of FMD assessment did not require vessel uncovering and was combined with evaluation of acetylcholine-induced response in one MRI protocol, which allowed attainment of functional responses from 2 different vessels in response to different stimuli during one, short MRI-based set of measurements.

In addition to the assessment of endothelium-dependent vasodilation, the MRI-based method was used for the quantification of endothelial permeability using an operator-independent method to quantify results based on the Npx50 parameter, as described previously,[20] and a specially designed gadolinium-rich liposome preparation as contrast agents used herein for the first time. Most gadolinium-based MRI contrast agents, which can be used for detection of increased endothelial permeability, are small, nontargeted compounds that passively penetrate into the vascular wall with a broad nonspecific biodistribution[68] or gadolinium covalently bonded to albumin, allowing for higher, but still limited, vessel wall enhancement.[19,20] Liposomes of small size (110 nm) loaded with gadolinium used in the present

work allowed for good MRI-based detection of changes in endothelial permeability.[55] Altogether, simultaneous assessment of endothelium-dependent vasodilation in 3 arteries in response to acetylcholine or flow, together with quantification of endothelial permeability by MRI in vivo, an approach used in the present work, provided a unique insight into endothelial function in vivo in ApoE/LDLR$^{-/-}$ mice.

To confirm that impairment of endothelial function, assessed by MRI in vivo, is linked to impaired NO-dependent function, NO production in aorta ex vivo was measured by EPR,[47] the only analytical method that detects endothelial NO production directly, not indirectly. In addition to providing a broader view on early pathophysiological characteristics of endothelial dysfunction in ApoE/LDLR$^{-/-}$ mice, biomarkers of glycocalyx disruption (SDC-1 and ESM-1), endothelial inflammation (sVCAM-1, sICAM-1 and sE-sel), endothelial permeability (Angpt-2 and sFLT-1), and hemostasis (vWF, t-PA, and PAI-1) were simultaneously measured using the microLC/MS-MRM–based method, recently developed by our group.[44–46]

Finally, nanomechanical properties of the endothelium in ex vivo aorta were examined using spectroscopy by nanoindentation with an AFM tip[69–71] using a novel method of AFM nanoindentation-based detection of glycocalyx degradation and endothelial stiffness described previously by Targosz-Korecka et al.[31]

Such a multimodal approach for the comprehensive assessment of endothelial phenotype in vivo, supplemented by ex vivo analyses used in the present work, enabled an unprecedented insight into the temporal association of alterations in various aspects of endothelial phenotype, including glycocalyx integrity, endothelial stiffness, NO-dependent endothelial function, and other features of endothelial inflammation and dysfunction, usually analyzed separately, not simultaneously.[24,25,30,72]

In the present work, we evaluated the endothelial phenotype, in 4- to 8-week-old ApoE/LDLR$^{-/-}$ mice, at the stage before occurrence of the well-defined atherosclerotic plaque compared with 28-week-old mice, and at the stage of advanced atherosclerotic plaque development. Although we identified early changes in smooth muscle cells and intima, we confirmed that atherosclerotic plaques were absent in the BCA up to the age of 10 weeks using scrupulous analysis of the proximal, middle, and distal parts of the BCA and originally developed staining with OMSB, providing reliable color contrast to distinguish numerous constituents of atherosclerotic plaque.[61] These results are in accordance with the work of Csányi et al,[28] showing that well-defined atherosclerotic plaques in ApoE/LDLR$^{-/-}$ mice fed a standard diet do not occur before the age of 12 weeks.

In previous studies, endothelial dysfunction, assessed as impaired NO-mediated relaxation in ex vivo vascular preparations, was repeatedly demonstrated in murine models of atherosclerosis.[23–25] However, it was not a universal finding in ApoE$^{-/-}$ mice,[27] and some authors claimed that endothelial dysfunction occurs only at the late stage of the development of atherosclerotic plaques in this model.[24,26] We previously demonstrated that the impairment of NO-dependent relaxation in the aorta, measured in a classic vascular preparation setup, was present in 8-week-old ApoE/LDLR$^{-/-}$ mice, a model characterized by a robust hypercholesterolemia with increased total, low-density lipoprotein, and high-density lipoprotein cholesterol levels.[28]

In the present work, to our surprise, the complex multifactorial nature of endothelial dysfunction was revealed as early as in 4- to 8-week-old ApoE/LDLR$^{-/-}$ mice, significantly before the occurrence of the well-defined atherosclerotic plaque. At this early stage of endothelial response to hypercholesterolemic insult, the dysfunctional phenotype involved diminished glycocalyx coverage and lengths and endothelial stiffness. These factors coincided with the impairment of endothelium-dependent vasodilation and NO-dependent function, increased endothelial permeability, and increased plasma concentration of biomarkers of glycocalyx disruption (ESM-1), endothelial inflammation (sVCAM-1), vascular permeability (Angpt-2), and hemostasis (PAI-1 and t-PA). The multimodal approach adopted in the present work was useful to show that early impairment of endothelium-dependent vasodilation (by MRI) in the aorta was confirmed by impaired NO production in the aorta (by EPR), whereas glycocalyx injury in the aorta (by AFM) was supported by increased biomarkers of glycocalyx disruption (ESM-1). Increased endothelial permeability (by MRI) was confirmed by increased plasma concentration of Angpt-2. The evaluation of endothelial inflammation and hemostasis was based on biomarker analysis only (changes in sVCAM-1, t-PA, and PAI-1). Taken together, the results presented herein suggest that endothelial dysfunction in atherosclerosis, even at the early stage before the occurrence of the well-defined atherosclerotic plaque, is a complex multifactorial phenomenon that has not been previously appreciated.

The important question arises about whether these divergent manifestations of endothelial dysfunction, including glycocalyx disruption and various features of endothelial dysfunction, appear in sequence or more likely, their co-occurrence is rather indicative for vicious circle relations, as suggested recently for impaired endothelial glycocalyx, endothelial mechanotransduction, and NO-dependent function.[63] For example, silencing of glypican-1 or SDC-1 was shown to inhibit shear stress–induced activation of endothelial NO synthase,[73] while replenishment of glycocalyx improved mechanoactivation-induced NO generation.[63] Increased endothelial cortical stiffness may impair flow-mediated NO production, and NO production seems to be regulated by cortical stiffness.[73–77]

The reciprocal relation between impaired NO function and endothelial inflammation is rather well accepted because NO deficiency promoted increased expression of endothelial adhesion molecules, and vice versa.[78,79] Deterioration of glycocalyx resulted in increased endothelial permeability[36,80,81]; in turn, endothelial barrier disruption is also linked to increased Angpt-2, which mediates breakdown of glycocalyx.[82] Glycocalyx damage also induces a proinflammatory endothelial response (eg after removal of the glycocalyx component SDC-1).[75] Clearly, glycocalyx shedding facilitated monocyte adhesion and infiltration, which promoted vascular inflammation, lipid retention, and the development of atherosclerotic plaques.[76] Furthermore, inhibition of hyaluronan synthesis (by 4-methylumbelliferone) facilitated leukocyte adhesion, subsequent inflammation, and progression of atherosclerosis.[40] In turn, leukocyte infiltration and subsequent vascular inflammation promoted extrinsic pathways of glycocalyx degradation by sheddases known to involve not only heparanase and hyaluronidase, but also matrix metalloproteinases activated in endothelial inflammation: thrombin, plasmin involved in thrombotic and fibrinolytic processes, elastase, and proteinase 3 released by endothelium-adherence leukocytes.[83] Interestingly, biglycan, a constituent of the glycocalyx of capillaries, inhibited thrombin activity, platelet activation, and, finally, macrophage-mediated plaque inflammation.[39] On the other hand, impaired endothelial glycocalyx promoted platelet adhesion to endothelium.[36]

Altogether, numerous mechanisms were previously identified, by which glycocalyx injury may contribute to impairment of NO-dependent function, increased endothelial permeability, endothelial stiffness, vascular inflammation, thrombosis and fibrinolysis, and atherosclerosis development; and these processes may reciprocally promote glycocalyx injury. Our results do not support the notion that glycocalyx injury proceeded other manifestations of endothelial dysfunction because glycocalyx injury coincided with all manifestations of endothelial dysfunction and all of them were detected as early as in 4- to 8-week-old ApoE/LDLR$^{-/-}$ mice, as though at this early stage, there was a full-blown phenotype of endothelial dysfunction. We have no experimental data to exclude that high hypercholesterolemia of ApoE/LDLR$^{-/-}$ mice induced some manifestations of endothelial dysfunction, including glycocalyx injury, before birth or within the first 4 weeks of maternal feeding; and then, others symptoms of endothelial dysfunction occurred progressively. However, given some feedback-forward reinforcement mechanisms between perturbed endothelial glycocalyx and progression of endothelial dysfunction that have been recently put forward,[63] we are rather tempted to support the notion of the complex multifactorial nature of early endothelial dysfunction that, to our knowledge, has not been previously appreciated.

Accordingly, the loss of endothelial glycocalyx integrity seems to be an integral part, but not a separate event, of endothelial dysfunction, as also suggested when studying endothelial response to acute hyperglycemia.[84]

Interestingly, in the present study, the earliest (in 4-week-old mice) changes in glycocalyx integrity were manifested as reduced glycocalyx coverage coexisting with increased endothelial stiffness, followed by reduction in the effective glycocalyx length (in 8-week-old mice). These results underscore a similar pattern of early changes in glycocalyx integrity in ApoE/LDLR$^{-/-}$ mice as in the db/db mouse model of diabetes mellitus, in which stiffening of endothelial cells and diminished glycocalyx coverage occurred in early diabetes mellitus and were followed by the reduction of the glycocalyx length that correlated with diabetes mellitus progression.[31] On the other hand, in ApoE/LDLR$^{-/-}$ mice, it was the changes in the glycocalyx coverage, not length, that were most progressively impaired in old compared with young ApoE/LDLR$^{-/-}$ mice. These differences may suggest that in atherosclerosis, intrinsic mechanisms of glycocalyx degradation linked to exocytosis of lysosome-related organelles and their cargo, with subsequent patchy loss of glycocalyx,[85] play an important role.

Our results have diagnostic and therapeutic significance. For an endothelial dysfunction diagnosis, interestingly, nearly all major features of endothelial dysfunction detected early remained altered, to an approximately similar extent, in the atherosclerotic phase in 28-week-old ApoE/LDLR$^{-/-}$ mice. The only exceptions were the occurrence of acetylcholine-induced vasoconstriction in the aorta and BCA, impaired flow-mediated vasodilation in the FA, and the progressive nature of reduction of glycocalyx length and coverage, with a concomitant further increase in endothelial permeability. Accordingly, only some of the features of endothelial dysfunction, including glycocalyx disruption and endothelial permeability, have a progressive nature in atherosclerosis; and those features, not others, may constitute a reliable measure of the progression of endothelial dysfunction.[30]

In terms of endothelium pharmacological characteristics, there are several drugs endowed with endothelial/vasoprotective activity that have been found to be important in the treatment of various diseases,[86,87] and there is increasing awareness of the endothelium as a novel attractive target for pharmacotherapy.[88] Given the complex nature of the early phase of endothelial dysfunction reported herein in atherosclerosis, it seems unlikely that the correction of the function of a single endothelial mechanism will be effective, unless restoring the one well-designed component of dysfunctional endothelial machinery will improve all the others. To date, the drugs that possess a broader spectrum of endothelial activity constitute the forefront of pharmacological characteristics of the endothelium, whereas some of the single-mechanism—based approaches failed.[89] Further

proof-of-concept studies are required to point out the effective ways to therapeutically achieve a reversal of a complex, multifactorial early response of endothelium to hypercholesterolemia.

There are limitations of this study that need to be underlined. First, in the present study, only female mice were used, making it impossible to study the impact of sex on early endothelial phenotype in mice with atherosclerosis. We assume that the early phase of endothelial dysfunction is a complex multifactorial response regardless of sex of the animals, but obviously sexual dimorphism may pertain to differences in endothelial phenotype. There are several studies addressing the molecular mechanisms of differences in endothelial function in female sex compared with male sex, in particular as regard to microvascular and resistance vessel function.[90]

Second, in the present study, the impairment of endothelium-dependent vasodilation was detected by MRI in vivo and was not compared with commonly performed assessment of endothelial dysfunction based on measurements of endothelial-dependent vasodilation in ex vivo isolated vessel preparation. To the best of our knowledge, there is no direct comparison of these 2 approaches to measure endothelial-dependent vasodilation. Thus, it remains to be determined whether the progression of endothelial dysfunction assessed by MRI in vivo, compared with the ex vivo approach, would give fully concordant results.

Third, we reported that multiple manifestations of endothelial dysfunction occur simultaneously in 4-week-old ApoE/LDLR$^{-/-}$ mice. However, it cannot be excluded that high hypercholesterolemia of ApoE/LDLR$^{-/-}$ mice induces some features of endothelial dysfunction before birth or within the first 4 weeks of maternal feeding, and there is a sequence of events that we could not determine, as in our study we characterized 4-week-old mice, but not younger mice.

Conclusion

Taking advantage of the unique and comprehensive armamentarium of in vivo and ex vivo methods, including functional 3D MRI-based assays of endothelial phenotype and AFM-based measurements of glycocalyx degradation and endothelial stiffening, we demonstrated herein, to our knowledge for the first time, that in 4- to 8-week-old ApoE/LDLR$^{-/-}$ mice at the stage proceeding development of the well-defined atherosclerosis, the dysfunctional phenotype of endothelium involves diminished glycocalyx coverage and length. These factors coincide with but do not proceed the impairment of endothelium-dependent vasodilation and NO-dependent function, increased endothelial permeability, and increased plasma concentration of biomarkers of glycocalyx disruption (ESM-1), endothelial inflammation (sVCAM-1), vascular

permeability (Angpt-2), and hemostasis (PAI-1 and t-PA). These results underscore the fact that endothelial dysfunction, even at the early stage, is a complex multifactorial response. Our findings have pathophysiological as well as diagnostic and therapeutic significance.

Sources of Funding

Disclosures

None.

References

1. Blann AD. Assessment of endothelial dysfunction: focus on atherothrombotic disease. *Pathophysiol Haemost Thromb*. 2003;33:256–261.

2. Davignon J, Ganz P. Role of endothelial dysfunction in atherosclerosis. *Circulation*. 2004;109:III27–III32.

3. Anderson TJ, Gerhard MD, Meredith IT, Charbonneau F, Delagrange D, Creager M, Selwyn P, Ganz P. Systemic nature of endothelial dysfunction in atherosclerosis. *Am J Cardiol*. 1995;75:71B–74B.

4. Dharmashankar K, Widlansky ME. Vascular endothelial function and hypertension: insights and directions. *Curr Hypertens Rep*. 2010;12:448–455.

5. Marti CN, Gheorghiade M, Kalogeropoulos AP, Georgiopoulou VV, Quyyumi AA, Butler J. Endothelial dysfunction, arterial stiffness, and heart failure. *J Am Coll Cardiol*. 2012;60:1455–1469.

6. Franses JW, Drosu NC, Gibson WJ, Chitalia VC, Edelman ER. Dysfunctional endothelial cells directly stimulate cancer inflammation and metastasis. *Int J Cancer*. 2013;133:1334–1344.

7. Flammer AJ, Anderson T, Celermajer DS, Creager MA, Deanfield J, Ganz P, Hamburg NM, Lüscher TF, Shechter M, Taddei S, Vita JA, Lerman A. The assessment of endothelial function: from research into clinical practice. *Circulation*. 2012;126:753–767.

8. Halcox JPJ, Schenke WH, Zalos G, Mincemoyer R, Prasad A, Waclawiw MA, Nour KRA, Quyyumi AA. Prognostic value of coronary vascular endothelial dysfunction. *Circulation*. 2002;106:653–658.

9. Schachinger V, Britten MB, Zeiher AM. Prognostic impact of coronary vasodilator dysfunction on adverse long-term outcome of coronary heart disease. *Circulation*. 2000;101:1899–1906.

10. Ludmer PL, Selwyn AP, Shook TL, Wayne RR, Mudge GH, Alexander RW, Ganz P. Paradoxical vasoconstriction induced by acetylcholine in atherosclerotic coronary arteries. *N Engl J Med*. 1986;315:1046–1051.

11. Wilkinson IB, Webb DJ. Venous occlusion plethysmography in cardiovascular research: methodology and clinical applications. *Br J Clin Pharmacol*. 2001;52:631–646.

12. Brant LC, Barreto SM, Passos VM, Ribeiro AL. Reproducibility of peripheral arterial tonometry for the assessment of endothelial function in adults. *J Hypertens*. 2013;31:1984–1990.

13. Dupouy P, Geschwind HJ, Pelle G, Gallot D, Dubois-Randé JL. Assessment of coronary vasomotion by intracoronary ultrasound. *Am Heart J*. 1993;126:76–85.

14. Raitakari OT, Celermajer DS. Flow-mediated dilatation. *Br J Clin Pharmacol*. 2000;50:397–404.

15. Frolow M, Drozdz A, Kowalewska A, Nizankowski R, Chlopicki S. Comprehensive assessment of vascular health in patients: towards endothelium-guided therapy. *Pharmacol Rep*. 2015;67:786–792.

16. Bonetti PO, Pumper GM, Higano ST, Holmes DR, Kuvin JT, Lerman A. Noninvasive identification of patients with early coronary atherosclerosis by assessment of digital reactive hyperemia. *J Am Coll Cardiol*. 2004;44:2137–2141.

17. Lee JMS, Shirodaria C, Jackson CE, Robson MD, Antoniades C, Francis JM, Wiesmann F, Channon KM, Neubauer S, Choudhury RP. Multi-modal magnetic resonance imaging quantifies atherosclerosis and vascular dysfunction in patients with type 2 diabetes mellitus. *Diab Vasc Dis Res*. 2007;4:44–48.

18. Leeson CP, Robinson M, Francis JM, Robson MD, Channon KM, Neubauer S, Wiesmann F. Cardiovascular magnetic resonance imaging for non-invasive assessment of vascular function: validation against ultrasound. *J Cardiovasc Magn Reson*. 2006;8:381–387.

19. Phinikaridou A, Andia ME, Protti A, Indermuehle A, Shah A, Smith A, Warley A, Botnar RM. Noninvasive magnetic resonance imaging evaluation of endothelial permeability in murine atherosclerosis using an albumin-binding contrast agent. *Circulation*. 2012;126:707–719.

20. Bar A, Skorka T, Jasinski K, Sternak M, Bartel Ż, Tyrankiewicz U, Chlopicki S. Retrospectively-gated MRI for in vivo assessment of endothelium-dependent vasodilatation and endothelial permeability in murine models of endothelial dysfunction. *NMR Biomed*. 2016;29:1088.

21. Bar A, Olkowicz M, Tyrankiewicz U, Kus E, Jasinski K, Smolenski RT, Skorka T, Chlopicki S. Functional and biochemical endothelial profiling in vivo in a murine model of endothelial dysfunction: comparison of effects of 1-methylnicotinamide and angiotensin-converting enzyme inhibitor. *Front Pharmacol*. 2017;8:183.

22. Sternak M, Bar A, Adamski MG, Mohaissen T, Marczyk B, Kieronska A, Stojak M, Kus K, Tarjus A, Jaisser F, Chlopicki S. The deletion of endothelial sodium channel α (αENaC) impairs endothelium-dependent vasodilation and endothelial barrier integrity in endotoxemia in vivo. *Front Pharmacol*. 2018;9:178.

23. Bonthu S, Heistad DD, Chappell DA, Lamping KG, Faraci FM. Atherosclerosis, vascular remodeling, and impairment of endothelium-dependent relaxation in genetically altered hyperlipidemic mice. *Arterioscler Thromb Vasc Biol*. 1997;17:2333–2340.

24. Crauwels HM, Van Hove CE, Holvoet P, Herman AG, Bult H. Plaque-associated endothelial dysfunction in apolipoprotein E-deficient mice on a regular diet: effect of human apolipoprotein AI. *Cardiovasc Res*. 2003;59:189–199.

25. Laursen JB, Somers M, Kurz S, McCann L, Warnholtz A, Freeman BA, Tarpey M, Fukai T, Harrison DG. Endothelial regulation of vasomotion in apoE-deficient mice: implications for interactions between peroxynitrite and tetrahydrobiopterin. *Circulation*. 2001;103:1282–1288.

26. Yang R, Powell-Braxton L, Ogaoawara AK, Dybdal N, Bunting S, Ohneda O, Jin H. Hypertension and endothelial dysfunction in apolipoprotein E knockout mice. *Arterioscler Thromb Vasc Biol*. 1999;19:2762–2768.

27. Villeneuve N, Fortuno A, Sauvage M, Fournier N, Breugnot C, Jacquemin C, Petit C, Gosgnach W, Carpentier N, Vanhoutte P, Vilaine J-P. Persistence of the nitric oxide pathway in the aorta of hypercholesterolemic apolipoprotein-E-deficient mice. *J Vasc Res*. 2003;40:87–96.

28. Csányi G, Gajda M, Franczyk-Zarow M, Kostogrys R, Gwóźdź P, Mateuszuk L, Sternak M, Wojcik L, Zalewska T, Walski M, Chlopicki S. Functional alterations in endothelial NO, PGI2 and EDHF pathways in aorta in ApoE/LDLR$^{-/-}$ mice. *Prostaglandins Other Lipid Mediat*. 2012;98:107–115.

29. Walczak M, Suraj J, Kus K, Kij A, Zakrzewska A, Chlopicki S. Towards a comprehensive endothelial biomarkers profiling and endothelium-guided pharmacotherapy. *Pharmacol Rep*. 2015;67:771–777.

30. Mitra R, O'Neil GL, Harding IC, Cheng MJ, Mensah SA, Ebong EE. Glycocalyx in atherosclerosis-relevant endothelium function and as a therapeutic target. *Curr Atheroscler Rep*. 2017;19:63.

31. Targosz-Korecka M, Jaglarz M, Malek-Zietek KE, Gregorius A, Zakrzewska A, Sitek B, Rajfur Z, Chlopicki S, Szymonski M. AFM-based detection of glycocalyx degradation and endothelial stiffening in the db/db mouse model of diabetes. *Sci Rep*. 2017;7:15951.

32. Sieve I, Münster-Kühnel AK, Hilfiker-Kleiner D. Regulation and function of endothelial glycocalyx layer in vascular diseases. *Vascul Pharmacol*. 2018;100:26–33.

33. Davies PF. Flow-mediated endothelial mechanotransduction. *Physiol Rev*. 1995;75:519–560.

34. Hsieh H-J, Liu C-A, Huang B, Tseng AH, Wang D. Shear-induced endothelial mechanotransduction: the interplay between reactive oxygen species (ROS) and nitric oxide (NO) and the pathophysiological implications. *J Biomed Sci*. 2014;21:3.

35. Manchanda K, Kolarova H, Kerkenpaß C, Mollenhauer M, Vitecek J, Rudolph V, Kubala L, Baldus S, Adam M, Klinke A. MPO (myeloperoxidase) reduces endothelial glycocalyx thickness dependent on its cationic charge. *Arterioscler Thromb Vasc Biol*. 2018;38:1859–1867.

36. Curry FE, Adamson RH. Endothelial glycocalyx: permeability barrier and mechanosensor. *Ann Biomed Eng*. 2012;40:828–839.

37. Schött U, Solomon C, Fries D, Bentzer P. The endothelial glycocalyx and its disruption, protection and regeneration: a narrative review. *Scand J Trauma Resusc Emerg Med*. 2016;24:48.

38. Reitsma S, Oude Egbrink M, Heijnen V, Megens R, Engels W, Vink H, Slaaf DW, van Zandvoort M. Endothelial glycocalyx thickness and platelet-vessel wall interactions during atherogenesis. *Thromb Haemost*. 2011;106:939–946.

39. Grandoch M, Kohlmorgen C, Melchior-Becker A, Feldmann K, Homann S, Müller J, Kiene L-S, Zeng-Brouwers J, Schmitz F, Nagy N, Polzin A, Gowert NS, Elvers M, Skroblin P, Yin X, Mayr M, Schaefer L, Tannock LR, Fischer JW. Loss of biglycan enhances thrombin generation in apolipoprotein E-deficient mice: implications for inflammation and atherosclerosis. *Arterioscler Thromb Vasc Biol*. 2016;36:e41–e50.

40. Nagy N, Freudenberger T, Melchior-Becker A, Rock K, ter Braak M, Jastrow H, Kinzig M, Lucke S, Suvorava T, Kojda G, Weber AA, Sorgel F, Levkau B, Ergun S, Fischer JW. Inhibition of hyaluronan synthesis accelerates murine atherosclerosis: novel insights into the role of hyaluronan synthesis. *Circulation*. 2010;122:2313–2322.

41. Tarbell JM, Pahakis MY. Mechanotransduction and the glycocalyx. *J Intern Med*. 2006;259:339–350.

42. Oberleithner H, Peters W, Kusche-Vihrog K, Korte S, Schillers H, Kliche K, Oberleithner K. Salt overload damages the glycocalyx sodium barrier of vascular endothelium. *Pflügers Arch*. 2011;462:519–528.

43. Givens C, Tzima E. Endothelial mechanosignaling: does one sensor fit all? *Antioxid Redox Signal*. 2016;25:373–388.

44. Suraj J, Kurpińska A, Olkowicz M, Niedzielska-Andres E, Smolik M, Zakrzewska A, Jasztal A, Sitek B, Chlopicki S, Walczak M. Development, validation and application of a micro–liquid chromatography–tandem mass spectrometry based method for simultaneous quantification of selected protein biomarkers of endothelial dysfunction in murine plasma. *J Pharm Biomed Anal*. 2018;149:465–474.

45. Suraj J, Kurpińska A, Sternak M, Smolik M, Niedzielska-Andres E, Zakrzewska A, Sacha T, Kania A, Chlopicki S, Walczak M. Quantitative measurement of selected protein biomarkers of endothelial dysfunction in plasma by micro-liquid chromatography-tandem mass spectrometry based on stable isotope dilution method. *Talanta*. 2019;194:1005–1016.

46. Suraj J, Kurpińska A, Zakrzewska A, Sternak M, Stojak M, Jasztal A, Walczak M, Chlopicki S. Early and late endothelial response in breast cancer metastasis in mice: simultaneous quantification of endothelial biomarkers using mass spectrometry-based method. *Dis Model Mech*. 2019; Jan 25. pii: dmm.036269.

47. Przyborowski K, Proniewski B, Czarny J, Smeda M, Sitek B, Zakrzewska A, Zoladz JA, Chlopicki S. Vascular nitric oxide–superoxide balance and thrombus formation after acute exercise. *Med Sci Sports Exerc*. 2018;50:1405–1412.

48. Ishibashi S, Herz J, Maeda N, Goldstein J, Brown M. The two-receptor model of lipoprotein clearance: tests of the hypothesis in "knockout" mice lacking the low density lipoprotein receptor, apolipoprotein E, or both proteins. *Proc Natl Acad Sci USA*. 1994;10:4431–4435.

49. Kostogrys RB, Franczyk-Zarow M, Gasior-Glogowska M, Kus E, Jasztal A, Wrobel TP, Baranska M, Czyzynska-Cichon I, Drahun A, Manterys A, Chlopicki S. Anti-atherosclerotic effects of pravastatin in brachiocephalic artery in comparison with en face aorta and aortic roots in ApoE/LDLR$^{-/-}$ mice. *Pharmacol Rep*. 2017;69:112–118.

50. Tyrankiewicz U, Skorka T, Orzylowska A, Jablonska M, Jasinski K, Jasztal A, Bar A, Kostogrys R, Chlopicki S. Comprehensive MRI for the detection of subtle alterations in diastolic cardiac function in apoE/LDLR$^{-/-}$ mice with advanced atherosclerosis. *NMR Biomed*. 2016;29:833–840.

51. Mateuszuk L, Jasztal A, Maslak E, Gasior-Glogowska M, Baranska M, Sitek B, Kostogrys R, Zakrzewska A, Kij A, Walczak M, Chlopicki S. Antiatherosclerotic effects of 1-methylnicotinamide in apolipoprotein E/low-density lipoprotein receptor-deficient mice: a comparison with nicotinic acid. *J Pharmacol Exp Ther*. 2016;356:514–524.

52. Wrobel TP, Marzec KM, Chlopicki S, Maślak E, Jasztal A, Franczyk-Żarów M, Czyżyńska-Cichoń I, Moszkowski T, Kostogrys RB, Baranska M. Effects of low carbohydrate high protein (LCHP) diet on atherosclerotic plaque phenotype in ApoE/LDLR$^{-/-}$ mice: FT-IR and Raman imaging. *Sci Rep*. 2015;5:14002.

53. Kostogrys RB, Franczyk-Żarów M, Maślak E, Gajda M, Mateuszuk Ł, Jackson CL, Chłopicki S. Low carbohydrate, high protein diet promotes atherosclerosis in apolipoprotein E/low-density lipoprotein receptor double knockout mice (apoE/LDLR$^{-/-}$). *Atherosclerosis*. 2012;223:327–331.

54. Langbein H, Brunssen C, Hofmann A, Cimalla P, Brux M, Bornstein SR, Deussen A, Koch E, Morawietz H. NADPH oxidase 4 protects against development of endothelial dysfunction and atherosclerosis in LDL receptor deficient mice. *Eur Heart J*. 2016;37:1753–1761.

55. Przybylo M, Langner M, Borowik T. High-efficiency encapsulation of hydrophilic compounds in unilamellar liposomes. International Patent Application PCT/EP2018/057400. International Publication WO 2018/172504 A1. 2018 LIPID SYSTEMS SP. Z.O.O. [PL/PL]; ul. Krzemieniecka 48C 54-613 Wroclaw, PL.

56. Cheng HL, Wright GA. Rapid high-resolution T1 mapping by variable flip angles: accurate and precise measurements in the presence of radiofrequency field inhomogeneity. *Magn Reson Med*. 2006;55:566–574.

57. Wang J, Qiu M, Kim H, Constable RT. T1 measurements incorporating flip angle calibration and correction in vivo. *J Magn Reson*. 2006;182:283–292.

58. Bar A, Skorka T, Jasinski K, Chlopicki S. MRI-based assessment of endothelial function in mice in vivo. *Pharmacol Rep*. 2015;67:765–770.

59. Sokolov I, Dokukin ME, Guz NV. Method for quantitative measurements of the elastic modulus of biological cells in AFM indentation experiments. *Methods*. 2013;60:202–213.

60. Depre C, Havaux X, Renkin J, Vanoverschelde JL, Wijns W. Expression of inducible nitric oxide synthase in human coronary atherosclerotic plaque. *Cardiovasc Res*. 1999;41:465–472.

61. Gajda M, Jasztal A, Banasik T, Jasek-Gajda E, Chlopicki S. Combined orcein and martius scarlet blue (OMSB) staining for qualitative and quantitative analyses of atherosclerotic plaques in brachiocephalic arteries in apoE/LDLR$^{-/-}$ mice. *Histochem Cell Biol*. 2017;147:671–681.

62. Noble MIM, Drake-Holland AJ, Vink H. Hypothesis: arterial glycocalyx dysfunction is the first step in the atherothrombotic process. *QJM*. 2008;101:513–518.

63. Zhang X, Sun D, Song JW, Zullo J, Lipphardt M, Coneh-Gould L, Goligorsky MS. Endothelial cell dysfunction and glycocalyx—a vicious circle. *Matrix Biol*. 2018;71–72:421–431.

64. Price AN, Cheung KK, Cleary JO, Campbell AE, Riegler J, Lythgoe MF. Cardiovascular magnetic resonance imaging in experimental models. *Open Cardiovasc Med J*. 2010;4:278–292.

65. Schuler D, Sansone R, Freudenberger T, Rodriguez-Mateos A, Weber G, Momma TY, Goy C, Altschmied J, Haendeler J, Fischer JW, Kelm M, Heiss C. Measurement of endothelium-dependent vasodilation in mice: brief report. *Arterioscler Thromb Vasc Biol*. 2014;34:2651–2657.

66. Machin DR, Leary ME, He Y, Shiu Y-T, Tanaka H, Donato AJ. Ultrasound assessment of flow-mediated dilation of the brachial and superficial femoral arteries in rats. *J Vis Exp*. 2016; Nov 3;(117).

67. Song W, Zhou L, Kot KL, Fan H, Han J, Yi J. Measurement of flow-mediated dilation of mouse femoral artery in vivo by optical coherence tomography. *J Biophotonics*. 2018;11:e201800053.

68. Caravan P, Ellison JJ, McMurry TJ, Lauffer RB. Gadolinium(III) chelates as MRI contrast agents: structure, dynamics, and applications. *Chem Rev*. 1999;99:2293–2352.

69. Szczygiel AM, Brzezinka G, Targosz-Korecka M, Chlopicki S, Szymonski M. Elasticity changes anti-correlate with NO production for human endothelial cells stimulated with TNF-α. *Pflugers Arch*. 2012;463:487–496.

70. Bai K, Wang W. Spatio-temporal development of the endothelial glycocalyx layer and its mechanical property in vitro. *J R Soc Interface*. 2012;9:2290–2298.

71. Hayashi K, Higaki M. Stiffness of intact endothelial cells from fresh aortic bifurcations of atherosclerotic rabbits: atomic force microscopic study. *J Cell Physiol*. 2017;232:7–13.

72. Dinh QN, Chrissobolis S, Diep H, Chan CT, Ferens D, Drummond GR, Sobey CG. Advanced atherosclerosis is associated with inflammation, vascular dysfunction and oxidative stress, but not hypertension. *Pharmacol Res*. 2017;116:70–76.

73. Ebong EE, Lopez-Quintero SV, Rizzo V, Spray DC, Tarbell JM. Shear-induced endothelial NOS activation and remodeling via heparan sulfate, glypican-1, and syndecan-1. *Integr Biol (Camb)*. 2014;6:338–347.

74. Tzima E, Irani-Tehrani M, Kiosses WB, Dejana E, Schultz DA, Engelhardt B, Cao G, DeLisser H, Schwartz MA. A mechanosensory complex that mediates the endothelial cell response to fluid shear stress. *Nature*. 2005;437:426–431.

75. Voyvodic PL, Min D, Liu R, Williams E, Chitalia V, Dunn AK, Baker AB. Loss of syndecan-1 induces a pro-inflammatory phenotype in endothelial cells with a dysregulated response to atheroprotective flow. *J Biol Chem*. 2014;289:9547–9559.

76. Kusche-Vihrog K, Callies C, Fels J, Oberleithner H. The epithelial sodium channel (ENaC): mediator of the aldosterone response in the vascular endothelium? *Steroids*. 2010;75:544–549.

77. Warnock DG, Kusche-Vihrog K, Tarjus A, Sheng S, Oberleithner H, Kleyman TR, Jaisser F. Blood pressure and amiloride-sensitive sodium channels in vascular and renal cells. *Nat Rev Nephrol*. 2014;10:146–157.

78. De Caterina R, Libby P, Peng HB, Thannickal VJ, Rajavashisth TB, Gimbrone MA, Shin WS, Liao JK, Liao JK. Nitric oxide decreases cytokine-induced endothelial activation: nitric oxide selectively reduces endothelial expression of adhesion molecules and proinflammatory cytokines. *J Clin Invest*. 1995;96:60–68.

79. Khan BV, Harrison DG, Olbrych MT, Alexander RW, Medford RM. Nitric oxide regulates vascular cell adhesion molecule 1 gene expression and redox-sensitive transcriptional events in human vascular endothelial cells. *Proc Natl Acad Sci USA*. 1996;93:9114–9119.

80. Rahbar E, Cardenas JC, Baimukanova G, Usadi B, Bruhn R, Pati S, Ostrowski SR, Johansson PI, Holcomb JB, Wade CE. Endothelial glycocalyx shedding and vascular permeability in severely injured trauma patients. *J Transl Med*. 2015;13:117.

81. Becker BF, Chappell D, Jacob M. Endothelial glycocalyx and coronary vascular permeability: the fringe benefit. *Basic Res Cardiol*. 2010;105:687–701.

82. Lukasz A, Hillgruber C, Oberleithner H, Kusche-Vihrog K, Pavenstädt H, Rovas A, Hesse B, Goerge T, Kümpers P. Endothelial glycocalyx breakdown is mediated by angiopoietin-2. *Cardiovasc Res*. 2017;113:671–680.

83. Dogné S, Flamion B, Caron N. Endothelial glycocalyx as a shield against diabetic vascular complications: involvement of hyaluronan and hyaluronidases. *Arterioscler Thromb Vasc Biol*. 2018;38:1427–1439.

84. Nieuwdorp M, Mooij HL, Kroon J, Atasever B, Spaan JAE, Ince C, Holleman F, Diamant M, Heine RJ, Hoekstra JBL, Kastelein JJP, Stroes ESG, Vink H. Endothelial glycocalyx damage coincides with microalbuminuria in type 1 diabetes. *Diabetes*. 2006;55:1127–1132.

85. Zullo JA, Fan J, Azar TT, Yen W, Zeng M, Chen J, Ratliff BB, Song J, Tarbell JM, Goligorsky MS, Fu BM. Exocytosis of endothelial lysosome-related organelles hair-triggers a patchy loss of glycocalyx at the onset of sepsis. *Am J Pathol*. 2016;186:248–258.

86. Daiber A, Di Lisa F, Ferdinandy P. Pharmacology of oxidative stress: translational opportunities. *Br J Pharmacol*. 2017;174:1511–1513.

87. Gryglewski RJ. Pharmacology of vascular endothelium. *FEBS J*. 2005;272:2956–2967.

88. Kiseleva RY, Glassman PM, Greineder CF, Hood ED, Shuvaev VV, Muzykantov VR. Targeting therapeutics to endothelium: are we there yet? *Drug Deliv Transl Res*. 2018;8:883–902.

89. Chłopicki S, Gryglewski RJ. Angiotensin converting enzyme (ACE) and HydroxyMethylGlutaryl-CoA (HMG-CoA) reductase inhibitors in the forefront of pharmacology of endothelium. *Pharmacol Rep*. 2005;57(suppl):86–96.

90. Davel AP, Lu Q, Moss ME, Rao S, Anwar IJ, DuPont JJ, Jaffe IZ. Sex-specific mechanisms of resistance vessel endothelial dysfunction induced by cardiometabolic risk factors. *J Am Heart Assoc*. 2018;7:e007675. DOI: 10.1161/JAHA.117.007675.

SUPPLEMENTAL MATERIAL

Figure S1. AFM nanoindentation maps and automatic data classification results obtained for endothelium from ApoE/LDLR$^{-/-}$ and C57BL/6 mice
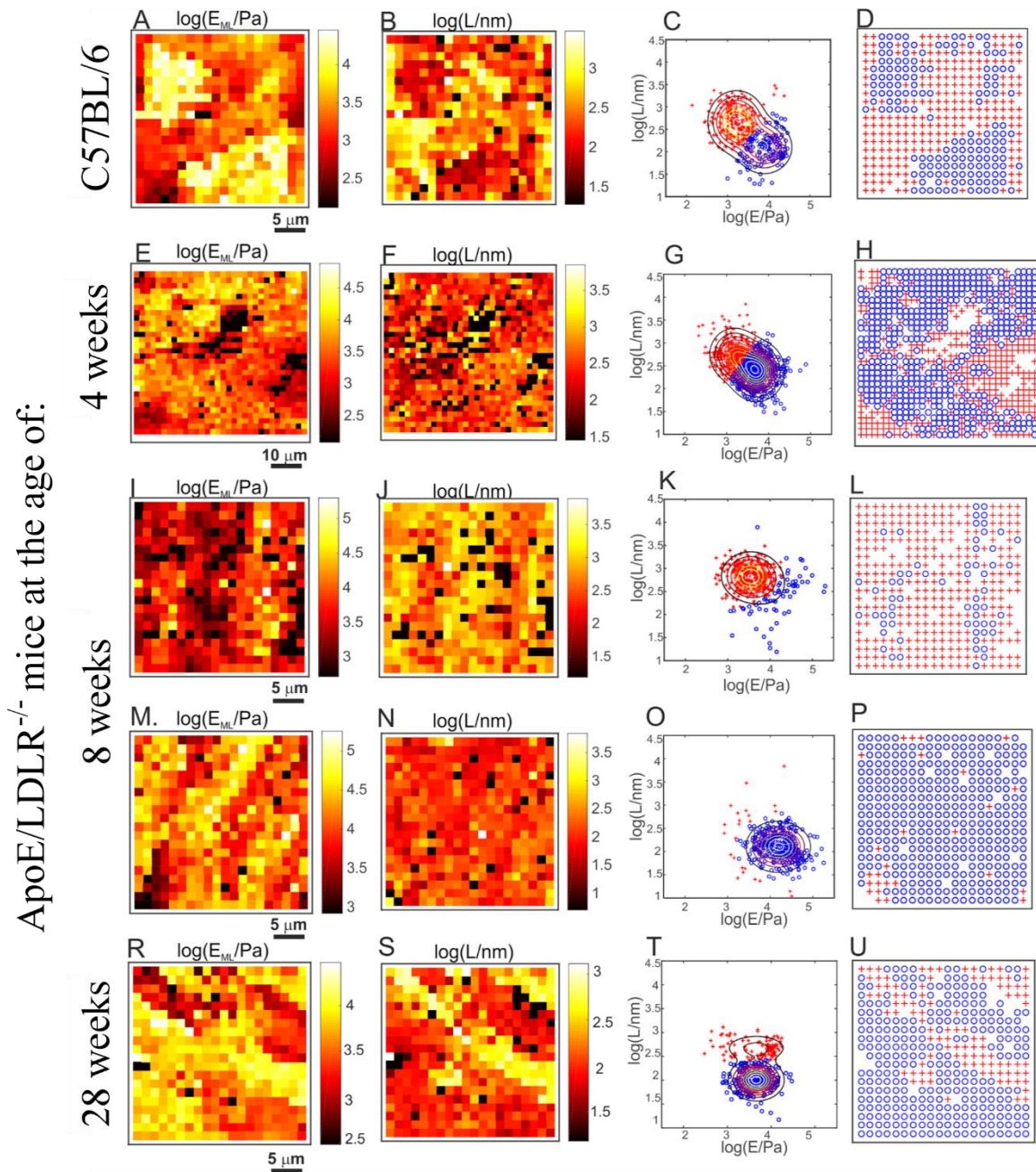
First row: Data for an 8-week-old control C57BL/6 mouse (C57BL/6). Second row: data for a 4-week-old ApoE/LDLR$^{-/-}$ mouse (4 weeks). Third and fourth row: data for an 8-week-old ApoE/LDLR$^{-/-}$ mouse (8 weeks). Fifth row: data for a 28-week-old ApoE/LDLR$^{-/-}$ mouse. (**A,E,I,M,R**) Values of the apparent elastic modulus derived from fragments of indentation curves near the maximum load E$_{ML}$. (**B,F,J,N,S**) Values of the glycocalyx length L. (**C,G,K,O,T**) Scatter plots showing values of the apparent elastic modulus values E$_{ML}$ and glycocalyx length L. Gaussian mixture distributions with two components were fitted to the data. Data points shown using

red crosses and blue circles were classified using an automatic clustering procedure as regions with and without the glycocalyx, respectively. (**D,H,L,P,U**). Spatial maps of glycocalyx distribution. Red crosses indicate endothelium covered with glycocalyx and blue circles indicate endothelium without glycocalyx brush. In all images, a large heterogeneity of mechanical properties and glycocalyx distribution of the samples can be observed.

Changes in nanomechanical parameters and glycocalyx coverage of the endothelium in ex vivo aorta in ApoE/LDLR^{-/-} mice

Figure S1 presents selected examples of AFM nanoindentation maps and data classification results obtained for abdominal aorta samples from control C57Bl/6 mice at age of eight weeks and from ApoE/LDLR^{-/-} mice at the ages of four, eight and twenty eight weeks. The spatial maps of the elasticity modulus and glycocalyx length revealed a massive heterogeneity of the aorta's surface. Therefore, all values presented on the spatial maps were transformed to a base 10 logarithmic scale. The spatial maps recorded for control C57Bl/6 mice revealed two well-resolved regions with significantly different values of the elastic modulus. In 'soft' regions with low values of elastic modulus, one can observe larger values of the glycocalyx length. In 'hard' regions (yellow colour in the false colour scale maps of E_{ML}), higher values of the elastic modulus correlate with shorter lengths of the glycocalyx. The results of the classification procedure are presented in **Fig. S1 C-D**. The scatter plots shown in **Fig. S1 C** reveal that data are grouped into two distinct components. The blue data points are classified as type of indentation curves acquired on the parts of endothelial cells without a glycocalyx, and the red data points are classified as indentation curves measured for the regions of endothelium covered with the glycocalyx surface layer. **In Fig. S1 D**, the results of the classification procedure are presented in the form of a spatial map. In this map, the red and blue points form well-resolved regions that correspond to endothelium covered by glycocalyx or without the glycocalyx brush. Contrary to the control sample, the spatial maps from **Fig. S1 E,F** measured for the 4-week-old mice revealed a significant spreading of the 'hard' regions (large values of EML and small values of L), which are identified as regions without the

glycocalyx. The quantitative classification confirmed our observations and showed a significant decrease of the glycocalyx coverage. Importantly, the data recorded for the 8-week-old mice reveal two types of spatial maps that represent different coverage of the endothelium with glycocalyx. For this sample, the maps shown in **Fig. S1 I-P**, are dominated by much larger regions with or without glycocalyx that fill the entire image. In the spatial map from **Fig. S1 L,** there are only few points recorded without glycocalyx and in **Fig. S1 P** the endothelium surface is almost entirely depleted of glycocalyx. Moreover, while in both maps the elastic modulus values are higher than for the control sample (**Fig. S1 I and M**), the glycocalyx length (**Fig. S1 J**) remains at the level characteristic of the control sample. The spatial maps from **Fig. S1 R, S** measured for the 28-week-old mice revealed a significant increase of regions which were identified as 'stiff' regions without the glycocalyx. The quantitative classification (**Fig. S1 T,U**) showed a significant decrease of the curve classified as a curves with glycocalyx which corresponds to reduction of the glycocalyx coverage.

Figure S2. Representative images of BCA cross-sections stained with Unna's orcein combined with Martius, Scarlet and Blue trichrom (OMSB) in 8-week-old ApoE/LDLR^{-/-} mice.
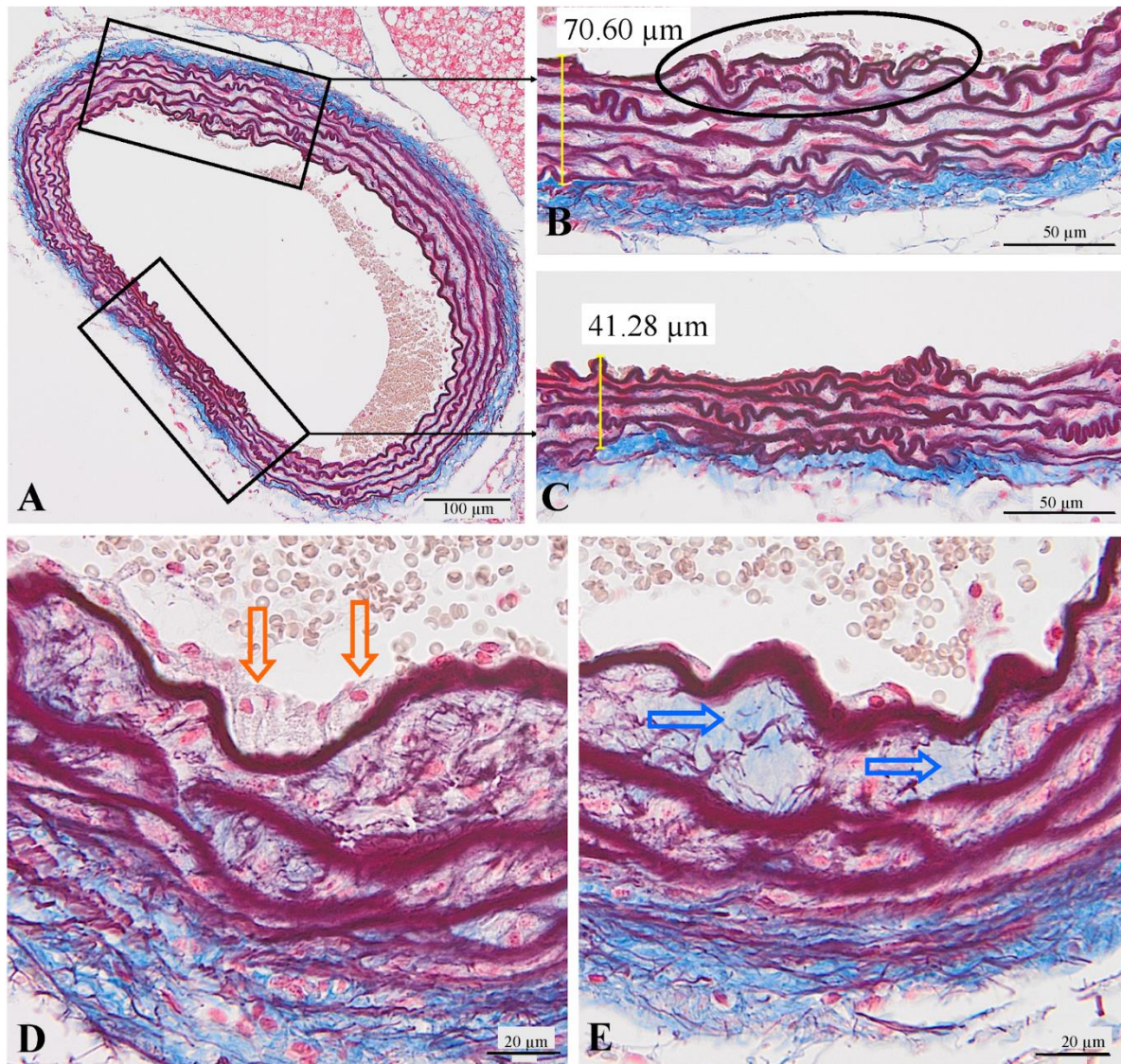
(**A**) Cross-section of BCA in middle part, showing changes in vessel wall (**B**) in comparison to appropriate part of the vessel wall (**C**), prior to well-defined atherosclerotic plaque development. Distance between elastic laminas and subendothelial layer were enlarged with evidence of smooth muscle cells migrating into the intima (**B,** black ellipse**).** Images showing the most pronounced monocyte adhesion found at analysed samples of BCA for 8-week-old ApoE/LDLR-/- mice (**D,** orange arrows), and most pronounced extracellular matrix depositing of collagen (**E,** blue arrows)**. As shown in Fig 5, in BCA from** 8-week-old ApoE/LDLR^{-/-} mice based on automatic quantification, the value of plaque/IVA was < 1% but still > 0%. This result was attributed to thickened intima, but not to well-defined atherosclerotic plaques because the plaque area was counted based on the area enclosed by the most internal elastic lamina of the BCA wall.